Selective synthesis of a valuable unsaturated fatty alcohol via catalytic and non-catalytic liquid-phase methyl oleate reduction

Alejandro Vallejo Orrego[1], Cristian Ferretti[2], and Verónica Díez[1]

[1]INCAPE
[2]IQAL

February 22, 2024

Abstract

The upgrading of oleyl alcohol synthesis via methyl oleate reduction using NaBH4 without H2 supply was investigated. It was possible to synthesize selectively the valuable unsaturated fatty alcohol with high yields. Non-catalytic and catalytic experiments were developed trying to improve the low final oleyl alcohol yield previously obtained. The effect of reaction temperature, methyl oleate/NaBH4 molar ratio and properties of different catalysts on final oleyl alcohol yield was analyzed. Thus, alumina-supported metal (M) catalysts (M = Fe, Ce, Mo) were synthesized by impregnation at incipient wetness. The M/Al2O3 catalysts were characterized in their chemical, textural, structural and acid-base properties using ICP, N2 physisorption, XRD and NH3 and CO2 TPD. During non-catalytic methyl oleate reduction final methyl oleate conversion and oleyl alcohol yield of 94% were obtained using a methyl oleate/NaBH4 molar ratio of 0.11 at 333 K. Catalytic activity of M/Al2O3 solids did not correlate with basic site number but increased as acid site number and ionic potential of M cations increase. This suggests that cations with high acid site number and polarizing power are the ones that promote the polarization of the ester C=O and anion [BH4]- bonds favoring de methyl oleate conversion. In addition, the reaction mechanism for fatty acid methyl ester reduction was investigated from a theoretical approach using Density Functional Theory method at B3LYP/6-31++G(d,p) computational level. Results obtained during theoretical calculations confirmed that the formation of reducing alcoxyborohydride species is energetically favored and allowed to understand the events at microscopic level involved in the reaction mechanism.

Highlights:

- Final oleyl alcohol yields up to 94% are obtained through non-catalytic catalytic experiments during methyl oleate reduction without the supply of H_2

- A temperature of 333 K and a methyl oleate/$NaBH_4$ molar ratio of 0.11 result the optimized conditions for oleyl alcohol synthesis

- Metal-based catalysts with high acid site number and polarizing power favor oleyl alcohol synthesis

- A DFT modeling of mechanism reaction confirm the analysis carried out at macroscopic level based on experimental results

- Theoretical calculations confirm that formation of reducing methoxyborohydride species is energetically favored

Natural fatty alcohol synthesis

methyl oleate (MO)

methanol

NaBH$_4$
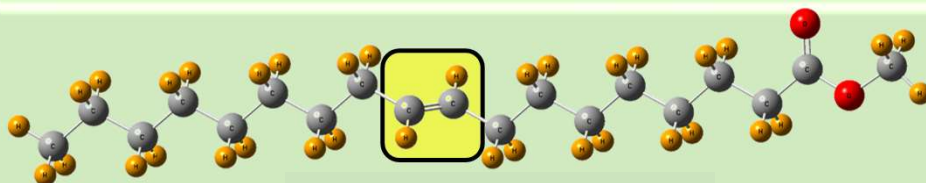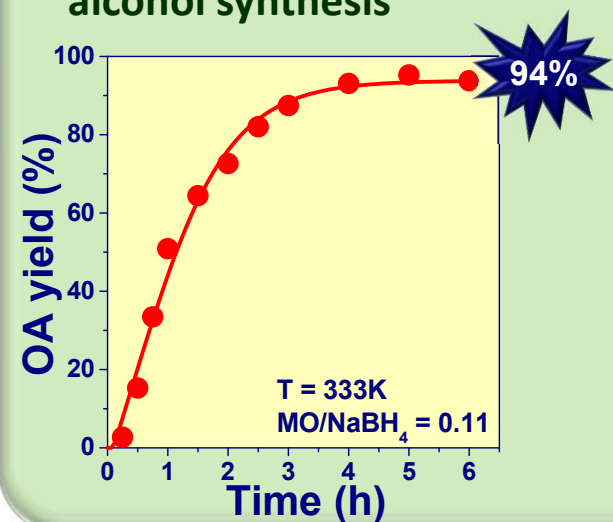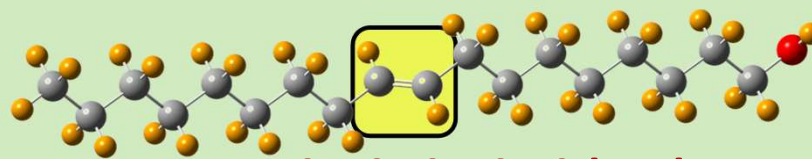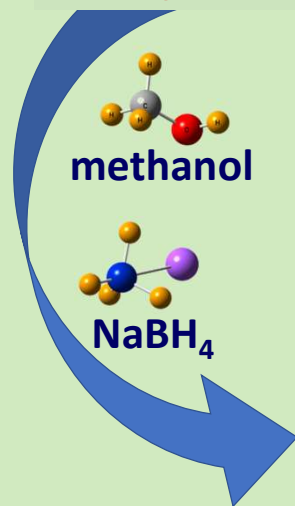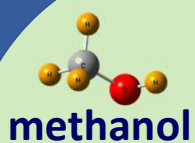
oleyl alcohol (OA)

OA uses

94%

OA yield (%)

Time (h)

T = 333K
MO/NaBH$_4$ = 0.11

2

3

4

5   **"Selective synthesis of a valuable unsaturated fatty alcohol via catalytic**

6   **and non-catalytic liquid-phase methyl oleate reduction"**

7

8

9   *By*

10

11   *Alejandro Vallejo Orrego [a], Cristián A. Ferretti [b] and Verónica K. Díez [a]**

12

13

14

15   [a] Catalysis Science and Engineering Research Group (GICIC), Research Institute of

16   Catalysis and Petrochemistry (INCAPE), UNL-CONICET, CCT CONICET Santa Fe,

17   Colectora Ruta Nac. 168, km 0, Paraje "El Pozo", (3000) Santa Fe, Argentina

18

19   [b] Fester Laboratory of Organic Chemistry, Institute of Applied Chemistry of Litoral,

20   IQAL, UNL-CONICET, Santiago del Estero 2829, (3000) Santa Fe, Argentina

21

22

23   *Corresponding author. Tel.: +54 342 4511546, Ex 6118; Fax: +54 342 4511170.

24   E-mail address: verodiez@fiq.unl.edu.ar (V.K. Díez).

Abstract

The upgrading of oleyl alcohol synthesis via methyl oleate reduction using $NaBH_4$ without H_2 supply was investigated. It was possible to synthesize selectively the valuable unsaturated fatty alcohol with high yields. Non-catalytic and catalytic experiments were developed trying to improve the low final oleyl alcohol yield previously obtained. The effect of reaction temperature, methyl oleate/$NaBH_4$ molar ratio and properties of different catalysts on final oleyl alcohol yield was analyzed. Thus, alumina-supported metal (M) catalysts (M = Fe, Ce, Mo) were synthesized by impregnation at incipient wetness. The M/Al_2O_3 catalysts were characterized in their chemical, textural, structural and acid-base properties using ICP, N_2 physisorption, XRD and NH_3 and CO_2 TPD. During non-catalytic methyl oleate reduction final methyl oleate conversion and oleyl alcohol yield of 94% were obtained using a methyl oleate/$NaBH_4$ molar ratio of 0.11 at 333 K. Catalytic activity of M/Al_2O_3 solids did not correlate with basic site number but increased as acid site number and ionic potential of M cations increase. This suggests that cations with high acid site number and polarizing power are the ones that promote the polarization of the ester C=O and anion $[BH_4]^-$ bonds favoring de methyl oleate conversion. In addition, the reaction mechanism for fatty acid methyl ester reduction was investigated from a theoretical approach using Density Functional Theory method at B3LYP/6-31++G(d,p) computational level. Results obtained during theoretical calculations confirmed that the formation of reducing alcoxyborohydride species is energetically favored and allowed to understand the events at microscopic level involved in the reaction mechanism.

Keywords: **methyl oleate; oleyl alcohol; sodium borohydride; reduction reaction mechanism; DFT calculations**

1. Introduction

Natural fatty alcohols (FOL) are linear, monohydric, saturated or unsaturated carbon compounds and have carbon chains between C6-C22. These fatty alcohols are obtained from renewable sources such as animal or vegetable fats, waxes and oils. Fatty alcohols, due to their amphiphilic character (combination of nonpolar carbon chain with polar hydroxyl group), exhibit surface and interface activity, which allows their use in emulsions and microemulsions [Noweck, 2011], favoring their use in personal care and cosmetic industries taking part in the formulation of liquid soaps, shampoos, conditioners, skin emollients, emulsifiers and densifiers of creams and lotions. Thus, fatty alcohols are employed in ionic and non-ionic surfactant production [Sad et al., 2007]. In particular, fatty alcohol sulfates and fatty alcohol ether sulfates belong to the group of anionic surfactants. In addition, fatty alcohol polyglycolethers and fatty alcohol ethoxilates are the first non-ionic surfactants manufactured in technical scale, being the ethoxilates compounds better low-foaming surfactants than the former. Alkyl polyglucosides are manufactured from fatty alcohols and sugar molecules following various procedures. These FOL-derived surfactants are surface active agents which have wide industrial applications as cleaning agents and detergents.

Industrially, natural FOL are synthetized by conversion of fatty acid methyl esters (FAME) and fatty acids (FA) via catalytic hydrogenation reaction. In these processes severe reaction conditions are used that involve high temperatures (473-573 K), high pressures of H_2 (20-30 MPa), and solid catalysts based mainly on chromium, such as Cu-Cr [Miya, 1981] and Zn-Cr [Rieke et al., 1997; Rieke et al., 1997], which resulted selective to FOL but is harmful to the environment due to the pollution generated by the final disposal of Cr. Due that, in recent years research has been directed at studying catalysts with similar catalytic activities, which are more efficient and generate less

75 pollution, mainly using catalysts based on noble metals. In fact, when using Ru-Sn/Al$_2$O$_3$

76 bimetallic catalysts, a high FOL selectivity is obtained by hydrogenation of methyl laurate

77 using milder reaction conditions (523 K, 5.6 MPa of H$_2$) [Toba et al., 1999]. In addition,

78 other authors using a similar Ru-Sn/Al$_2$O$_3$ catalyst, obtained stearyl alcohol (saturated

79 alcohol) with final yields up to 96% by hydrogenation of C=C and C=O bonds of methyl

80 oleate under severe reaction conditions (553 K, 10 MPa of H$_2$) [Tahara et al., 1996]. On

81 the other hand, when hydrogenating fatty acids (decanoic acid) over Re$_2$O$_7$, low

82 conversions and moderate selectivities to 1-decanol are achieved using 403 K and 10 MPa

83 of H$_2$ [Yoshino et al., 1990]. There are excellent results in the synthesis of FOL via

84 hydrogenation of FAME or FA, however, expensive noble metal-based catalysts and high

85 temperatures and H$_2$ pressures are required.

86 On the other hand, FAME reductions using mild reaction conditions via hydrogen and

87 hydride transfer in the liquid phase and without supplying gaseous H$_2$ have been studied

88 using homogeneous catalysis and there is practically no information related to the use of

89 heterogeneous catalysis in these reaction processes. In this sense, different authors have

90 demonstrated that metal hydrides are efficient carbonyl compounds reducing agents in

91 presence of alcohols of short carbon chain [Soai et al., 1982; Soai et al., 1984; Brown et

92 al., 1982; Rajeswara Rao et al., 1987; Xu et al., 2010]. Brown et al. [Brown et al., 1982]

93 studied the conversion of ethyl caproate and ethyl benzoate using NaBH$_4$, LiAlH$_4$ and

94 Ca(BH$_4$)$_2$ and alcohols such as ethanol and 2-propanol. In addition, Soai et al. [Soai et al.,

95 1982; Soai et al., 1984] investigated the esters and lactones reduction employing NaBH$_4$

96 and different solvent mixtures (tert-butanol/methanol, tetrahydrofuran/methanol).

97 Rajeswara et al. [Rajeswara Rao et al., 1987] and Xu et al. [Xu et al., 2010] investigated

98 the synthesis of FOL from FAME using NaBH$_4$ or LiAlH$_4$ and methanol achieving final

99   FOL yields between 35-96%. Thus, high ester conversions and alcohol selectivities have

100   been obtained in all these studies.

101   In addition, in a previous work [Vallejo Orrego et al., 2020] we managed to selectively

102   synthesize different FOL during non-catalytic experiments using mild reaction conditions

103   via hydrogen transfer and hydride without supplying H_2 gas. These results allowed us to

104   determine the role played by the hydride donor (metal hydride) and the hydrogen donors

105   (short carbon chain alcohols) in the fatty acid methyl ester reduction. Particularly, we

106   investigated the effect of fatty acid methyl ester structure using methyl laurate (ML),

107   methyl myristate (MM) and methyl oleate (MO). Experiments were carried out at 323 K

108   employing molar ratios methanol/$NaBH_4$ and FAME/$NaBH_4$ of 6.0 and 0.36,

109   respectively, and $NaBH_4$/Al_2O_3 as reducing solid. Results obtained in that reaction

110   conditions showed that final ML and MM conversions varied between 90.8 and 93.0%

111   while MO final conversion resulted significantly lower (34.5%).

112   Taking into account these previous results, in the present work we report on results

113   obtained during the upgrading of oleyl alcohol synthesis via methyl oleate reduction using

114   $NaBH_4$ as reducing agent without H_2 supply. Our goal is to continue the research related

115   to the synthesis of oleyl alcohol by carrying out non-catalytic and catalytic experiments

116   trying to improve the low final FOL yield previously obtained. Thus, catalysts based on

117   different M metals (M = Fe, Ce, Mo) supported on γ-Al_2O_3 were synthesized,

118   characterized, and tested in the MO liquid phase reduction reaction. The effect of reaction

119   conditions and the presence of different catalysts on final oleyl alcohol yield were

120   analyzed. In addition, the mechanism of reaction steps involved in non-catalytic reduction

121   of methyl oleate with $NaBH_4$ was investigated from a theoretical approach using density

122   functional theory (DFT) method at B3LYP/6-31++G(d,p) computational level.

123

2. Materials and experimental procedures

2.1. Chemicals and solid materials

126   The commercial fatty acid methyl ester, methyl oleate (Sigma-Aldrich, 99%) was used

127 without further purification. Fatty alcohol, oleyl alcohol (Sigma-Aldrich, $\geq$ 99%) was

128 employed for identification purpose. Methanol (Cicarelli, 99.8%) was used without any

129 purification.

130   The external standard n-hexadecane (Sigma-Aldrich, 99%) and the solvent

131 tetrahydrofuran, THF (Biopack, $\geq$ 99%) were used during tests.

132   Sodium borohydride, $NaBH_4$ (analytical grade) was purchased from Biopack.

133

134 *2.2. Catalyst synthesis*

135   Alumina-supported metal catalysts (MO_x/Al_2O_3, with M = Ce, Fe, Mo), containing

136 around 8.0 wt.% of metal were prepared by incipient wetness impregnation of commercial

137 γ-Al_2O_3 Cyanamid Ketjen CK 300 with aqueous solutions of different metal precursors.

138 Metal precursors used were $Ce(NO_3)_3.6H_2O$ (Fluka, $\geq$ 99%), $Fe(NO_3)_3.9H_2O$ (Anedra,

139 99%) and $Na_2MoO_4.2H_2O$ (Merck, 98%), respectively. The catalyst precursors were

140 thermally treated in flowing air at 673 K during 5 h with the exception of the one

141 containing molybdenum that was treated at 773 K. Catalysts were denoted as *x*MAl,

142 where *x* is the metal content expressed in wt.%.

143   The γ-Al_2O_3 pellets were crushed and sieved retaining particles between 180-480μm.

144 The powdered alumina was thermally treated at 773 K in flowing air for 5 h to remove

145 adsorbed water before the impregnation procedures.

146

147 *2.3. Catalyst characterization*

148 BET surface areas (SA) of catalysts were measured by N_2 physisorption at 77 K using

149 an Autosorb Quantachrome 1-C sorptometer. After calcination, the chemical content of

150 metal was analyzed by inductively coupled plasma (ICP-OES).

151 The structural properties of solid materials were analyzed by X-Ray Diffraction (XRD)

152 technique using a Shimadzu XD-D1 instrument with nickel filtered Cu Kα radiations

153 between 10 and 80°.

154 Total acid site number (n_a, μmol/g) were determined by TPD of NH_3 preadsorbed at

155 373 K. Samples were thermally treated in Heat the corresponding calcination temperature

156 and then exposed to a 1.11% NH_3/He flow at 373 K during 30 min to enable surface

157 saturation. Weakly adsorbed NH_3 was removed by flushing with He. The temperature

158 was then increased at a rate of 10 K/min from 373 K to 593 K and kept constant for 1 h.

159 NH_3 concentration in the reactor effluent was monitored by a mass spectrometer (MS)

160 detector in a Baltzers Omnistar unit.

161 Total basic site number (n_b, μmol/g) were measured by temperature-programmed

162 desorption (TPD) of CO_2 preadsorbed at room temperature. Samples were pretreated in

163 situ in a N_2 flow at 773 K, cooled to room temperature, and then exposed to a flowing

164 mixture of 3% of CO_2/N_2 until surface saturation was achieved (5 min). Weakly adsorbed

165 CO_2 was removed by flushing in N_2. Finally, the temperature was increased to 773 K at

166 a ramp rate of 10 K/min. Desorbed CO_2 was converted in CH_4 on a methanation catalyst

167 (Ni/Kieselghur), then analyzed using a flame ionization detector (FID).

168

169 ***2.4. Experimental procedure for methyl oleate reduction***

170 Typical non-catalytic and catalytic reduction reactions of methyl oleate (MO) with

171 methanol and pure $NaBH_4$ and *x*MAl catalyst-supported $NaBH_4$ were carried out.

172 Reaction temperatures between 308 K and 333 K and atmospheric pressure were used in

173 a semi batch four-necked glass reactor. A solution of MO in tetrahydrofuran (THF)

174 solvent with FAME/THF = 0.017 (molar ratio) was firstly loaded in the reactor. The

175 reactor was permanently exposed to an inert gas stream (flowing N_2). The reaction

176 mixture was warmed up to the reaction temperature. Magnetic stirring (700 rpm) was

177 used. The absence of solubilization problems of MO in the THF solvent under the reaction

178 conditions used was evidenced in the experiments. Thus, a single phase was observed

179 once all the reactants were added to the reactor at the reaction temperatures used.

180 During typical catalytic test an amount of 0.7 g of sodium borohydride ($NaBH_4$) was

181 added so that the molar ratio FAME/$NaBH_4$ in the reactor was 0.28. After that, a volume

182 of 5 mL of methanol was added over a period of 1 h reaching a molar ratio

183 alcohol/$NaBH_4$=6.0. During the 6-hour experiments, 11 samples of ≈ 0.2 mL were

184 extracted from the reactor.

185 Product of reaction was identified using a Thermo Scientific Trace 1300 GC with a

186 Thermo Scientific TR-5MS capillary column coupled to a Thermo Scientific ISQ QD MS

187 unit. The analysis and quantification of reactants and product concentrations (C_j) were

188 done using a 7890A Agilent Technologies GC equipped with a FID detector and a

189 Supelcowax-10 30M capillary column. Response factors were calculated using solutions

190 containing weighted amounts of the different reactants (FAME, short carbon chain

191 alcohols) and products (FOL) and the standard (n-hexadecane) were injected in the GC.

192 Methyl oleate conversion (X_{MO}^t) was calculated as:

$$X_{MO}^t \ (\%) = \frac{n_{MO}^0 - n_{MO}^t}{n_{MO}^0} \cdot 100 \qquad \text{(Eq. 1)}$$

194 where n_{MO}^0 are the moles of methyl oleate initially loaded to reactor and n_{MO}^t are the

195 moles of MO at the reaction time t. Selectivities to products j (S_j^t) classically defined as

196 shown in Equation 2:

197
$$S_j^t(\%) = \frac{n_j^t}{n_{MO}^0 - n_{MO}^t} \cdot 100 \qquad \text{(Eq. 2)}$$

198   were calculated in practice according to Equation 3:

199
$$S_j^t\ (\%) = \frac{C_j^t}{\sum C_j^t} \cdot 100 \qquad \text{(Eq. 3)}$$

200   since $\frac{n_{MO}^0 - n_{MO}^t}{Volume} = \sum C_j^t$. In Equation 3, C_j^t is the concentration of product j at reaction

201   time t.

202   Product yields (Y_j^t) were calculated according to Equation 4:

203
$$Y_j^t\ (\%) = \frac{X_{MO}^t(\%)\ S_j^t\ (\%)}{100} \qquad \text{(Eq. 4)}$$

204   The initial methyl oleate conversion rate (r_{MO}^0, mol/hg$_{cat}$) was calculated from the

205   initial slope of the X_{MO} vs. time curve after multiplication by n_{MO}^0/W, according to:

206

207
$$r_{MO}^0 = \left[\frac{d\ X_{MO}}{d\ (\frac{tW}{n_{MO}^0})} \right]_{\frac{tW}{n_{MO}^0} = 0} \qquad \text{(Eq. 5)}$$

208

209   where n_{MO}^0 is the number of moles of methyl oleate in the reactor at t = 0 and W the

210   catalyst load.

211

212   ***2.5. Computational details for theoretical study of FOL synthesis mechanism***

213   Density functional theory (DFT) molecular orbital calculations were performed using

214   the B3LYP/6-31++G(d,p) level theory [Lee et al.,1988] with Gaussian 09 software

215   package [Frisch et al., 2016]. An initial conformational optimization was performed for

216   the reactants, products and transition state (TS) geometries to obtain the lowest energy

217   conformation.

218   The theoretical study of the reaction mechanism was carried out, optimizing the

219   reactants, products, transition states and intermediate states. Looking for the transition

220   states, the frequencies of the optimized structures were calculated in order to verify that

221   one of them is negative. We confirmed that all the reactants, intermediates, and products

222   have no imaginary frequencies whereas each transition state has only one imaginary

223   frequency. Energies values presented and discussed in this work are Gibbs free energies,

224   because Gibbs free energies include thermal correction to the electronic energies, as well

225   as the entropic factor.

226   For modeling purposes, a shorter saturated methyl ester, methyl acetate, was used as

227   FAME. Each reaction mechanism step that was studied is composed of reactants,

228   transition state, intermediate state and products. We treated the reaction in the gas phase

229   and all thermochemical parameters were calculated at 298 K and 1 atm.

230

231   **3.   Results and discussion**

232   *3.1. Catalyst characterization*

233   Pure Al_2O_3 and *x*MAl catalysts were characterized in their chemical, textural,

234   structural and acid-base properties. Results obtained are presented in Table 1. The

235   chemical analysis, carried out by ICP, shows that catalyst metal loadings vary between

236   7.0 and 8.9 wt.%, which are close to the desired nominal content (8.0 wt.%). All catalytic

237   solids exhibit surface areas (*SA*) lower than that of the alumina support (230 m^2/g) and

238   vary between 53 and 173 m^2/g. This result suggests a pore blockage produced by metallic

239   species added during impregnation preparation method.

240   Structural properties of the solids were analyzed by XRD technique and the results

241   obtained for all samples investigated are shown in Figure 1. The XRD analysis of 7.7FeAl

242   and 7.0CeAl catalysts, showed signals attributable to incipient crystalline phases of Fe_2O_3

243 (JCPDS-ICDD 34-192), $AlFeO_4$ (JCPDS-ICDD 84-2153) and CeO_2 (JCPDS-ICDD 81-

244 792), respectively, in addition to the amorphous phase of the γ-Al_2O_3 support. On the

245 other hand, diffractogram of 8.9MoAl do not show crystalline phases of Mo incorporated

246 on the γ-Al_2O_3 during impregnation, suggesting that the Mo species are dispersed on the

247 surface of the support even with contents close to 8.9 wt.%.

248 The surface acid and basic properties of the xMAl samples were investigated by CO_2

249 TPD and NH_3 TPD techniques, respectively. The desorption profiles of both probe

250 molecules are shown in Figure 2. The CO_2 TPD profiles (Figure 2A) show that most

251 solids exhibit a single desorption peak centered at low temperature (360-400 K). This

252 result suggests that their basicity is weak. The number of total basic sites (n_b, μmol/g)

253 was determined by integration of the CO_2 desorption profiles and are presented in Table

254 1. As can be seen, the n_b value of the γ-Al_2O_3 support is low (19 μmol/g), in agreement

255 with previously reported results [i Díez et al., 2003]. On the other hand, as expected, the

256 promotion of the support with metal cations with recognized Lewis acid properties, in

257 general decreases the basic properties of the solids (Table 1). In effect, in all cases n_b

258 values of xMAl are lower than that of alumina varying from 1 to 16 μmol/g.

259 On the other hand, the NH_3 TPD profiles (Figure 2B) exhibit a broad desorption peak

260 between 500-900 K indicates the presence of acid species that adsorb NH_3 with different

261 binding energies. Al_2O_3 support exhibits two peaks at 480 and 615 K, corresponding to

262 weak and strong acid sites, respectively. Solids 7.7FeAl and 7.0CeAl also exhibit two

263 desorption peaks at 585 and 833 K. These results suggest that xMAl catalytic solids

264 exhibit strong acidity. The total acid site number (n_a, μmol/g) was determined by

265 integration of the NH_3 desorption profiles and are presented in Table 1. All the solids

266 showed n_a values higher than that of the support (24 μmol/g).

267 The acid properties of Lewis nature of the solids caused by incorporation of M^{n+}

11

268   cations, were theoretically evaluated considering the ionic potential q/r (Table 1). This

269   parameter, defined as the quotient between the charge and the radius of each of the cations

270   [Bernal et al., 2008], takes the lowest value for 7.0CeAl sample and the highest for

271   8.9MoAl catalyst. Evidence that this parameter allows visualizing the acidity of the

272   catalysts is its relationship with the n_a values. In fact, in Figure 3 it can be seen that n_a

273   increases monotonically with q/r.

274   In summary, observing in Table 1 the results obtained during the characterization of

275   the acid-base properties and data taken from literature for 8.9MoAl [Inmanee et al., 2017],

276   results evident that within the series of xMAl catalysts investigated, 8.9MoAl exhibits the

277   highest Lewis acidity.

278

3.2. Non-catalytic reduction of methyl oleate using pure $NaBH_4$

280   In a previous work [Vallejo Orrego et al., 2020] we demonstrated that fatty alcohol

281   (FOL) synthesis can be performed through non-catalytic fatty acid methyl ester (FAME)

282   reduction experiments without H_2 supply. Through these experiments it was possible to

283   elucidate the roles of $NaBH_4$ and methanol in FAME reduction. Both reactants allow

284   forming alkoxyborohydride species which are better reducing agents than $NaBH_4$. We

285   also postulated a mechanism for methyl laurate reduction and which is shown adapted for

286   any FAME in Scheme 1. The effect of FAME structure was also investigated in this

287   previous work employing methyl laurate (ML), methyl myristate (MM) and methyl oleate

288   (MO). Results obtained showed that the lowest final FAME conversion was achieved

289   using MO which barely reached 34.5%. As expected, the only FOL obtained from ML

290   and MM were lauryl alcohol and myristyl alcohol, respectively; i.e., the saturated FOL,

291   reaching in both cases selectivities of 100%. Surprisingly, using methyl oleate as starting

292   FAME oleyl alcohol was exclusively obtained, i.e., the selectivity towards unsaturated

293 FOL was 100%. This result allowed us to conclude that $NaBH_4/Al_2O_3$ contributes to the

294 selective reduction of C=O bond preserving C=C bond of MO.

295   In this work, the experiments are focused on optimization of the MO reduction reaction

296 using $NaBH_4$ as reducing agent (hydride donor) and methanol (proton donor). The MO

297 reduction reaction is shown in Scheme 2 where the stoichiometric ratio involved is

298 depicted. Our goal was to improve the low final MO conversion (X_{FAME}) and FOL yield

299 (Y_{FOL}) values obtained using MO as the starting FAME in our previous work [**¡Error!**

300 **Marcador no definido.** Vallejo Orrego et al., 2020].

301   The effect of reaction temperature on MO conversion and FOL yield was firstly

302 investigated. These experiments were carried out using typical methanol/$NaBH_4$ and

303 FAME/$NaBH_4$ molar ratios of 6.0 and 0.28, respectively. Figure 4 shows the MO

304 conversion evolution with reaction time obtained at 308, 320 and 333 K. In all

305 experiments, selectivity towards unsaturated FOL (oleyl alcohol) was 100%. Results

306 from Figure 4 and Table 2 show an increase of final methyl oleate conversion (X_{MO}) and

307 final oleyl alcohol yield (Y_{OA}) as reaction temperature increases from 308 to 333 K. In

308 effect, the X_{MO} values reached at end of reaction (6 h) were 31.9, 40.2 and 58.6%,

309 respectively (Table 2). Reaction temperature can not be increased above 333 K working

310 at atmospheric pressure due that the boiling temperature of methanol co-reactant (338 K).

311   From the analysis of reaction temperature effect can be concluded that 333 K is the

312 most appropriate temperature to carried out MO reduction and it was adopted to perform

313 optimization of experimental conditions.

314   After optimizing the reaction temperature, the effect of MO/$NaBH_4$ molar ratio was

315 investigated. During these experiments pure $NaBH_4$, a molar ratio methanol/$NaBH_4$ of

316 6.0, MO/$NaBH_4$ molar ratios of 0.11, 0.28 and 0.72 and a reaction temperature of 333 K

317 were used. The evolution of MO conversion with reaction time for each MO/$NaBH_4$

318   molar ratio is shown in Figure 5. The oleyl alcohol (S_{OA}) was the only product observed

319   in all experiments. The best results were obtained working with an excess of $NaBH_4$

320   respect to the stoichiometric ratio 1:1 indicated in the reaction pathway of Scheme 2.

321   Results from Figure 5 also show that the higher the excess of the reducing agent, the

322   higher the final OA yield. In fact, results from Table 2 show that the final FOL yield

323   increases from 21.4% to 93.9% by decreasing the $MO/NaBH_4$ molar ratio from the 0.72

324   to 0.11.

325   In a previous work, we obtained similar results during reaction condition optimization

326   using methyl laurate (ML) as starting FAME [Vallejo Orrego et al., 2020] and in all

327   experiments. In those experiments, the selectivity toward FOL was 100% and ML

328   conversions at 6 h of reaction were 72, 78, and 98%, respectively.

329   The conversion of methyl oleate to fatty alcohols was previously studied. In most of

330   these works the reaction strategy is the catalytic hydrogenation using high pressures of

331   gaseous H_2 (0.1 and 8 MPa) and high temperatures (473-563 K). Thus, in some of them

332   expensive catalysts involving noble metals such as Ru-Sn/Al_2O_3 [Echeverri et al., 2011;

333   Pouilloux et al., 1996; Narasimhan et al., 1989; Mazzieri et al., 2010], Ru-Ge/Al_2O_3

334   [Sánchez et al., 2013] have been employed. Final yields toward unsaturated alcohol (oleyl

335   alcohol) were generally low and varied between 12 and 60% being the saturated FAME

336   (methyl stearate) and saturated alcohol (stearyl alcohol) the main products obtained.

337   Other authors used mono and bimetallic catalysts based in no-noble metals supported on

338   different oxides, such as Co/ZnO, Sn/ZnO, Co/Al_2O_3, Co-Sn/Al_2O_3, Co-Sn/ZnO, Co-

339   Sn/SiO_2 [Pouilloux et al., 1998; Pouilloux et al., 2000; De Oliveira et al., 2001; De

340   Oliveira et al., 2012]. Using these catalysts, MO hydrogenation yields mainly heavy esters

341   (oleyl oleate) being the yields toward oleyl alcohol low (11-51%).

342   Different authors investigated metal hydrides as effective reducing agents of C=O

343   compounds using short carbon chain alcohols [Soai et al., 1982; Soai et al., 1984; Brown

344   et al., 1982; Rajeswara Rao et al., 1987; Xu et al., 2010], but the raw materials to be

345   reduced in these cases were ethyl caproate and ethyl benzoate [Brown et al., 1982] using

346   different metal hydrides or esters and lactones using $NaBH_4$ [Soai et al., 1982; Soai et al.,

347   1984]. However, very few works are known in the open literature that have investigated

348   methyl oleate (MO) reduction using metal hydrides as reducing agents. In effect, McKee

349   et al. [McKee et al., 2019] and Xin et al. [Xin et al., 2021] investigated MO reduction

350   using cobalt chloride/sodium borohydride and Ni-La-B systems, respectively, but these

351   studies lead methyl stearate as main product (reduction of C=C bond) and not produce

352   the most value product (unsaturated alcohol). The best result during methyl oleate

353   reduction to the corresponding unsaturated FOL (oleyl alcohol, OA) using $NaBH_4$ or

354      $LiAlH_4$ and methanol was obtained by Rajeswara Rao et al. [Rajeswara Rao et al., 1987],

355   reaching a final yield toward oleyl alcohol of 72%. However, in these works authors do

356   not investigate fully the effect that different reaction conditions have on oleyl alcohol

357   selectivity and yield during MO reduction. Here, we achieved promising results during

358   the reduction reaction of methyl oleate to the unsaturated fatty alcohol (oleyl alcohol)

359   making for the first time, a huge effort in analyzing the effect of reaction conditions

360   during optimization of OA synthesis through non-catalytic MO reduction.

361

362   *3.3. Methyl oleate reduction using $NaBH_4$ supported on xMAl catalysts.*

363   In previous paragraphs the optimization of reaction conditions during oleyl alcohol

364   (OA) synthesis from methyl oleate (MO) using $NaBH_4$ and without supplying H_2 gas was

365   described. However, despite the high MO conversion values obtained at the end of the

366   reaction in experiments carried out at 333 K and whit a molar ratio $MO/NaBH_4$ of 0.11,

15

367   initial FAME conversion values were low, as we could be concluded analyzing the slopes

368   at the origin of the conversion vs. time curves of Figures 4 and 5.

369   Previously, a mechanism for the reduction of FAME in using $NaBH_4$ and methanol as

370   co-reactants was proposed [Vallejo Orrego et al., 2020]. Briefly, the initial stage of

371   mechanism consists in the formation of the reducing species: alkoxyborohydride anions.

372   The second stage involves the successive steps that allow the interaction between the

373   reducing species and the FAME, leading to the formation of FOL. FAME (MO)

374   conversion to FOL (OA) requires reducing species that allow the reduction of the C=O

375   carbonyl group of FAME. To do this, $NaBH_4$ interacts with methanol generating

376   alkoxyborohydride species $[BH_{4-n}(CH_3O)_n]^-$ (n = 1, 2, 3) that are more effective reducing

377   agents than the borohydride anion $[BH_4]^-$, as concluded from results obtained previously

378   [Vallejo Orrego et al., 2020]. This reducing effect increases each time a methoxy group

379   is attached to $[BH_4]^-$ species. After reducing species formation, MO is activated via the

380   interaction between C=O group and the dimethoxyborohydride anion. The hydride

381   addition of the reducing species originates a tetrahedral intermediate anion, which

382   immediately interacts with the B atom of an incipient species of $BH(OCH_3)_2$ through a

383   polar B-O bond. By subsequent removal of a methoxide specie, which is incorporated

384   into the dimethoxyborohydride anion, an aldehyde intermediate is formed, which rapidly

385   is reduced by interaction with the trimethoxyborohydride anion. Indeed, the H^- of the

386   reducing species attacks the carbon of the C=O group of the aldehyde leading to the

387   formation of a tetrahedral intermediate anion and the tetramethoxyborate species. In the

388   last part of mechanism, another methanol molecule protonates this tetrahedral

389   intermediate to form oleyl alcohol. In order to address the study of the mechanism from

390   a theoretical approach, slight modifications were made to the successive steps described

391   above, which will be described later.

392   Taking into account that postulated mechanism, metal cations have been incorporated

393   to Al_2O_3 before the incorporation of the co-reactant $NaBH_4$, and thus, xMAl catalysts

394   were synthesized. The goal was to increase the acidity and thus favor the polarization of

395   the C=O group of the ester and the $[BH_4]^-$ anion bond facilitating the formation of

396   reducing species and their attack on the C=O of the ester. The requirements of these metal

397   cations to favor polarization are: 1) to have a low ionic radius; 2) to possess high charge.

398   With this in mind, the 7.0CeAl, 7.7FeAl and 8.9MoAl catalysts were tested in the

399   reduction of MO to OA. Figure 6 shows the evolution of MO conversion with reaction

400   time on these solids, while Table 2 summarizes the final yields to OA (Y_{OA}) and the initial

401   conversion rates of FAME (r^0_{MO}) obtained. In all cases the selectivity to FOL were 100%.

402   The 8.9MoAl solid exhibits the highest final OA yield value. In fact, this catalyst reached

403   a Y_{OA} of 81.6% after 6 h reaction (Table 2), which is higher than the obtained on Al_2O_3

404   (Y_{OA} = 53.0%).

405   On the other hand, the reduction of MO on 7.0CeAl and 7.7FeAl catalysts allow to

406   obtain lower OA final yield (48.8% and 58.7%, respectively). This result confirms that,

407   in order to favor the bond polarization of the functional groups involved in the reaction,

408   small metallic cations with high charge are required, that is, high q/r values. On the other

409   hand, structural features, characterizes by XRD analysis (Figure 1 and Table 1), would

410   influence in catalytic results since xMoAl is the only catalyst where metal species are well

411   spread out on the surface of the support.

412   The effect of the surface acid-base properties and cation polarizing power (q/r

413   parameter) of xMAl solids on the catalytic activity was also investigated. In this way, the

414   initial MO conversion rate was related with n_b, n_a, and q/r. Results obtained are shown in

415   Figure 7A and 7B and Table 2. Results from Table 2 show that 8.9MoAl is the most active

416   catalysts during MO reduction. This was evidenced through its high value of r^0_{MO} (0.20

mol/hg), which favored a rapid formation of reducing species that concludes with obtaining the non-reducing anion $[B(OCH_3)_4]^-$ and therefore the Y_{OA} increases more slowly up to reach a final value of 81.6%. A similar behavior is exhibited by the 7.7FeAl catalyst, which showed high activity (Table 2) and therefore, the final Y_{OA} is rapidly reached after 2 h of reaction (Figure 6).

The catalytic activity of xMAl solids (r^0_{MO}) seems not to correlate clearly with n_b values, although apparently a maximum appears for 8.9MoAl catalyst (Figure 7A). In general, this result suggests that surface basic sites would not be directly involved in the conversion of MO to OA. On the other hand, Figure 7B clearly shows that r^0_{MO} values increase as n_a and q/r increase, suggesting that the M^{n+} cations whose nature have higher polarizing power (q/r values) and that are found in greater quantity on the surface of the catalyst (n_a values) are those that promote the polarization of the ester C=O and anion $[BH_4]^-$ bonds.
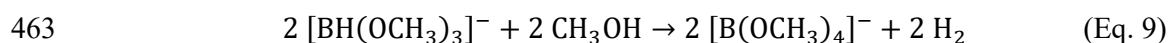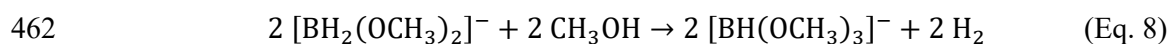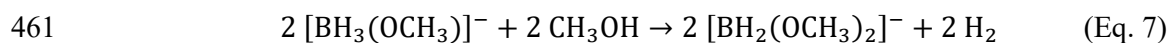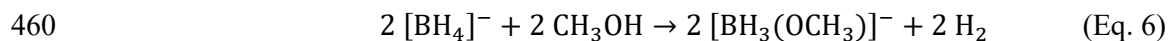
3.4. Molecular modeling by DFT of reaction steps involved in fatty alcohol synthesis

The reaction mechanism proposed for FAME reduction was studied from a theoretical approach. The molecular modeling was carried out optimizing reactants, products, transition states and intermediate states. During the search for the transition states (TS), the frequencies of the optimized structures were calculated in order to verify that one of them was negative. The result of this frequency was contrasted with the movement of the atoms involved in the reaction in order to confirm that this structure belonged to a transition state.

As previously mentioned, the calculations were made using methyl acetate as model molecule to represent FAME, whose reduction using $NaBH_4$ would lead toward ethanol (model molecule for FOL). The purpose of this choice is to decrease the size of the

442   calculations involved reducing both the time needed as well as the computational

443   resources. During calculations it was possible to establish a general balance of atoms

444   between reactants and products from the generation of the reducing species toward the

445   formation of the alcohol through interaction of FAME (methyl acetate) and

446   alkoxyborohydride species, and thus, was possible to normalize the free Gibbs energies

447   as a function of the energy of the initial reactants [Foresman et al., 2015] (ΔG, Kcal/mol).

448   In the first instance, the mechanism for reducing species (alcoxyborohydrides)

449   generation was evaluated, taking into account that in each step, methanol is part of the

450   reactants and there is hydrogen generation. In effect, the investigated methanolysis

451   reaction involves, two moles of borohydride anion $[BH_4]^-$ and eight moles of methanol

452   (CH_3OH) as starting reactants and two moles of tetramethoxyborate anion $[B(OCH_3)_4]^-$

453   and eight moles of hydrogen (H_2) as reaction products. The initial step of the global

454   mechanism for FAME reduction (also for methyl acetate) comprises a series of sub-steps

455   in which the anion $[BH_4]^-$ reacts with methanol through successive reactions to produce

456   initially the monosubstituted anion $[BH_3(OCH_3)]^-$ and hydrogen (Scheme 3), until the

457   fully substituted anion $[B(OCH_3)_4]^-$ is reached. The successive steps involved in

458   methanolysis reaction and used to perform the calculations are represented by Equations

459   6 to 9,

$$2\,[BH_4]^- + 2\,CH_3OH \rightarrow 2\,[BH_3(OCH_3)]^- + 2\,H_2 \qquad \text{(Eq. 6)}$$

$$2\,[BH_3(OCH_3)]^- + 2\,CH_3OH \rightarrow 2\,[BH_2(OCH_3)_2]^- + 2\,H_2 \qquad \text{(Eq. 7)}$$

$$2\,[BH_2(OCH_3)_2]^- + 2\,CH_3OH \rightarrow 2\,[BH(OCH_3)_3]^- + 2\,H_2 \qquad \text{(Eq. 8)}$$

$$2\,[BH(OCH_3)_3]^- + 2\,CH_3OH \rightarrow 2\,[B(OCH_3)_4]^- + 2\,H_2 \qquad \text{(Eq. 9)}$$

464   while Equation 10 represents the global methanolysis reaction of $[BH_4]^-$ of sodium

465   borohydride that has been widely discussed in the literature [Demirci et al., 2010;

466   Fernandes et al., 2009; Lo et al., 2007]:

467
$$2\,[BH_4]^- + 8\,CH_3OH \rightarrow 2\,[B(OCH_3)_4]^- + 8\,H_2 \qquad \text{(Eq. 10)}$$
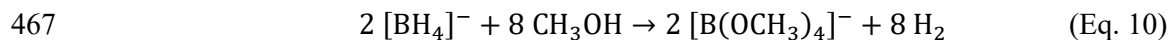
468   Since there is no information available about the coordinates of a structure that

469   represents a transition state that allows to simplify the calculations, a special strategy was

470   used to start the calculations. This strategy involves the use of synchronous quadratic

471   transit method (TSQ) [Foresman et al., 2015; Devia, 2018; Barroso, 2021] which consists

472   of finding a possible transition state from the coordinates of reactants, products and

473   optionally a third molecule corresponding to a supposed transition state. The coordinates

474   of the two reactants ($[BH_4]^-$ and methanol) and the two products ($[BH_3(OCH_4)]^-$ and

475   hydrogen) involved were first used, however, it failed to reach a satisfactory transition

476   state at negative energy and frequencies. Consequently, it was decided to build a pseudo-

477   transition state that resembled the reactants and products structures. Then, verifying the

478   presence of a single imaginary frequency and confirming that the energy of the structure

479   results higher than the energy of the reactants and products, this first structure was taken

480   as the basis for calculating the other transition states involved in methanolysis.

481   Figure 8A shows the initial optimized geometries of anionic borohydride species

482   $[BH_4]^-$, alkoxyborohydrides $[BH_{4-n}(OCH_3)_n]^-$ (n = 1, 2 and 3), tetramethoxyborate

483   $[B(OCH_3)_4]^-$ and the compounds methanol, methyl acetate, acetaldehyde and ethanol. In

484   addition, optimized structures obtained during the sub-steps of reaction pathway

485   presented in Scheme 3, including the corresponding transition state TS1, TS2, TS3 and

486   TS4, in which the bonds that are formed and broken are represented with dotted lines, are

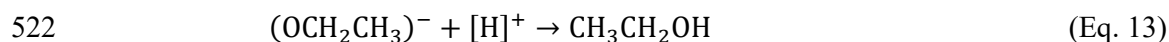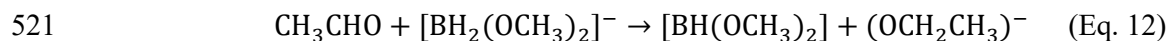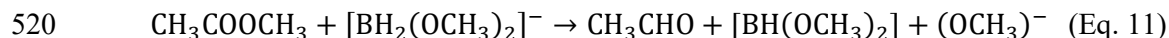487   presented in Figure 8B.

488   On the other hand, Figure 9 shows the progress of all steps involved in methyl acetate

489   reduction mechanism through the various intermediates and its different energy levels on

490   the potential energy diagram (PED), where the energy of the structures is represented as

491   a function of the reaction coordinate. Total Gibbs free energy of eight methanol

20

492   molecules, two $[BH_4]^-$ species, one hydrogen atom and one methyl acetate molecule has

493   been considered as the reference of the reaction in the energy profile ($\Delta G = 0$ Kcal/mol).
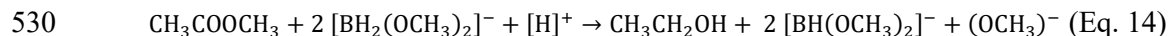
494   As can be seen, the formation of each alkoxyborohydride and tetramethoxyborate

495   species proceed spontaneously, i.e., they are reaction steps that are energetically favored

496   and therefore do not require an energy supply to be carried out. These results are

497   consistent with the experimental results presented in the literature on $[BH_4]^-$ methanolysis

498   [Ocon et al., 2013; Kaya et al., 2019]. The transition states found during the theoretical

499   study of the generation of reducing species have an imaginary frequency, the movement

500   of their atoms are consistent with formation of products and they have an energy higher

501   than the sum of the energies of the reactants or products. This allows us to conclude that

502   these structures correspond to the transition states (TS) of the reaction. In general, in the

503   transition states, the H^- from the borohydride or methoxyborohydride anion and the H^+

504   from methanol react to form gaseous hydrogen and the following substituted

505   alkoxyborohydride species. In conclusion, the results obtained in the generation of the

506   reducing species from theoretical calculations are in total agreement with the mechanism

507   proposed from experimental evidence in Scheme 1.

508   After studying, from a theorical point of view, the formation of the reducing species,

509   we evaluated the second part of the mechanism proposed in Scheme 1, which consists of

510   obtaining the fatty alcohol from the reduction of the ester. Considering that methyl acetate

511   is used as a model ester to represent FAME, the aldehyde that would be formed in the

512   first stage of the mechanism would be acetaldehyde and the alcohol that would be

513   generated as the final product would be ethanol. In order to simplify the analysis of the

514   interaction of reducing species with FAME (Scheme 1), to facilitate understanding of the

515   theoretical approach in the reaction pathway of Scheme 3 and taking into consideration

516   the time required to perform and analyze the results of the calculations, the theoretical

517   analysis that was carried out involves the species $[BH_2(OCH_3)_2]^-$ as unique reducing agent

518   of methyl acetate and acetaldehyde. Taking the above into account, Equations 11, 12 and

519   13 detail the sub-steps involved in the formation of ethanol.

520    $$CH_3COOCH_3 + [BH_2(OCH_3)_2]^- \rightarrow CH_3CHO + [BH(OCH_3)_2] + (OCH_3)^- \quad \text{(Eq. 11)}$$

521    $$CH_3CHO + [BH_2(OCH_3)_2]^- \rightarrow [BH(OCH_3)_2] + (OCH_2CH_3)^- \quad \text{(Eq. 12)}$$

522    $$(OCH_2CH_3)^- + [H]^+ \rightarrow CH_3CH_2OH \quad \text{(Eq. 13)}$$

523   Equation 11 represents the general expression to obtain the first intermediate of the

524   reaction, which corresponds to acetaldehyde for the model proposed in this study. As

525   shown in the Scheme 3, acetaldehyde in turn is rapidly reduced by $[BH_2(OCH_3)_2]^-$ species

526   or by another alkoxyborohydride species to form an ethoxide intermediate $(OCH_2CH_3)^-$

527   (Scheme 3), which is then converted to ethanol by H^+ from methanol. This last part of the

528   process is represented in Equations 12 and 13. General equation representing the whole

529   process is depicted in Equation 14:

530    $$CH_3COOCH_3 + 2\,[BH_2(OCH_3)_2]^- + [H]^+ \rightarrow CH_3CH_2OH + 2\,[BH(OCH_3)_2]^- + (OCH_3)^- \quad \text{(Eq. 14)}$$

531   In order to evaluate their energetic behavior and compare theoretical results of

532   calculations with the proposed experimental mechanism, frequencies of all the molecules

533   involved in each sub-step of the mechanism were calculated. For the TS5, TS6, TS7 and

534   TS8, the existence of an imaginary frequency (negative value) in the structures proposed

535   as a TS was verified.

536   Analysis of the results obtained in the theoretical calculation carried out on the

537   synthesis of ethanol was divided for a better understanding into two steps: formation of

538   the acetaldehyde intermediate and formation of the final product, ethanol.

539   To form acetaldehyde from methyl acetate, the presence of a nucleophilic compound

540   containing H^- ions is necessary to transfer electrons to the carbonyl group of the ester.

541   Results obtained are shown in Figures 8 and 9. The transition state TS5 is initially formed

542   from the attack of the anion $[BH_2(OCH_3)_2]^-$ to the C=O bond of methyl acetate (Figure

543   8B); then an intermediate (EI1 in Figure 8C) is formed in which the H^- forms a single

544   bond to the C=O group at the same time that the other single bond C-O between carbon

545   and the leaving group $(OCH_3)^-$ of methyl acetate begins to break, leaving the oxygen of

546   the C=O with negative charge. In the second transition state (TS6) formation, the C=O

547   bond is reformed and the $(OCH_3)^-$ group is lost (Scheme 3) leading to acetaldehyde

548     $[BH(OCH_3)_2]$ and $(OCH_3)^-$ species.

549   Figure 9 shows that the acetaldehyde formation results an exergonic reaction and is

550   energetically favored, since the products have a lower energy state (ΔG = -100.1

551   Kcal/mol) than the reactants (ΔG = -53.9 Kcal/mol).

552   The last part of ethanol formation mechanism requires the initial formation of an

553   ethoxide intermediate through reduction of acetaldehyde and then, the last step, involves

554   its conversion into ethanol (Scheme 3). The ethoxide formation (Equation 12) is

555   represented in Figure 8B while Figure 9 shows the energy profile as a function of the

556   reaction coordinate. As can be seen in Figure 8B, for the conversion of acetaldehyde (P5)

557   to ethoxide intermediate (EI2), a transition state (TS7) is formed in which a H^- of the

558   species $[BH_2(OCH_3)_2]^-$ attacks the carbon of acetaldehyde C=O group.

559   This approximation favors the breaking of alcoxyborohydride B-H bond and the

560   formation of the C-H bond that gives rise to ethoxide species. Ethoxide is considered an

561   intermediate between acetaldehyde and ethanol, in which the carbon atom of the C=O

562   group forms three bonds: two simple C-H bonds and other bond that corresponds to the

563   partial formation of a double bond between carbon and oxygen, in which the oxygen atom

564   meets delocalized electrons that would favor the formation of ethanol. Results presented

565   in Figure 9 show that the energy change involved in going from P5 to EI2 is not

566   energetically favored to form the ethoxide, indicating that this step requires extra energy

567 to be carried out. The fact that this structure is not energetically favored confirms that it

568 is a reaction intermediate state. The final sub-step of the reaction involves the formation

569 of ethanol (Equation 13). Calculation results obtained on this step are shown in Figures

570 8B and 9. To carry out the theoretical calculations in this sub-step, the H atom of methanol

571 was used as a proton source, which, as was verified in the theoretical studies of

572 methanolysis steps comes from the alcohol O-H group. On the other hand, in the

573 mechanism showed in Scheme 3, the H^+ of methanol participates in both the generation

574 of hydrogen and the alcohol formation. Thus, structures of Figure 8B show that in the

575 transition state (TS8), the H atom approaches the ethoxide to favor the formation of the

576 O-H bond leading to ethanol. Furthermore, in Figure 9 allow concluding that alcohol

577 formation occurs exergonically and thus, this sub-step is energetically favored.

578   In conclusion, the mechanism involved in the generation of reducing species was

579 theoretically elucidated. In this part of global mechanism, it was possible to confirm the

580 formation of alcoxyborohydride species is energetically favored. Furthermore, the results

581 obtained during the theoretical calculations for ethanol formation through methyl acetate

582 reduction, allowed us to understand the events at the microscopic level involved in the

583 mechanism of the reaction under study. In addition, the exhaustive study of the sub-steps

584 involved in the mechanism confirmed the formation of several structures

585 (alkoxyborohydride, acetaldehyde and ethoxide species) which act as intermediate

586 compounds in obtaining alcohol. Finally, reducing the size of the system in the theoretical

587 study allows to reach a first approach to the intermolecular interactions that exist between

588 the different species involved in the reduction of shorter ester than FAME; during

589 extrapolation of this theoretical study involving the synthesis of ethanol toward the

590 synthesis of fatty alcohols (FOL) derived from FAME, it was possible to confirm the

591   analysis carried out at macroscopic level (experimental results) by proposing in Scheme

592   1 the reaction mechanism for FOL synthesis.

593

594   **4. Conclusions**

595   Oleyl alcohol (OA) synthesis could be improved through non-catalytic and catalytic

596   experiments with selectivities of 100% from methyl oleate and methanol using both

597   unsupported $NaBH_4$ and catalyst-supported $NaBH_4$. In order to optimize the synthesis,

598   different reaction conditions (temperature, methyl oleate/$NaBH_4$ molar ratio and catalyst

599   nature) were employed without the supply of H_2 gaseous. Thus, in non-catalytic

600   experiments a final yield of the valuable unsaturated fatty alcohol OA of 93.9% was

601   achieved using a methyl oleate/$NaBH_4$ molar ratio of 0.11 and a reaction temperature of

602   333 K.

603   The effect of the incorporation of different metal cations M (M = Fe, Ce, Mo) to the

604   alumina support on the activity and OA yield was studied and it was found that

605    $8.9Mo/Al_2O_3$ solid, the catalyst with the highest acid site number and the highest

606   polarizing power, allow obtaining the best activity value. In fact, this catalytic solid favors

607   the C=O bond polarization of the ester and the anion $[BH_4]^-$ to form the actual reducing

608   species that then interact with the methyl oleate.

609   Reaction mechanism previously postulated for fatty acid methyl esters reduction

610   towards fatty alcohols using methanol and $NaBH_4$ was studied in this work from a

611   theoretical approach using density functional theory (DFT) method at B3LYP/6-

612   31++G(d,p) computational level. Calculations were made using methyl acetate as model

613   molecule to represent fatty acid methyl esters, whose reduction would lead toward ethanol

614   (model molecule for fatty alcohols). This choice allowed to decrease the size of the

615   calculations involved, reducing both the time needed as well as the computational

616   resources. It was possible to confirm that the formation of reducing alcoxyborohydride

617   species is energetically favored. On the other hand, results obtained during the theoretical

618   calculations for ethanol formation from methyl acetate, allowed to understand the events

619   at the microscopic level involved in the reaction mechanism studied. Finally, it was

620   possible demonstrate, that the reduction of the system size during the theoretical study

621   allows to reach a first approach to the intermolecular interactions that exist between the

622   different species involved in the acetate reduction. During extrapolation of the DFT study

623   performed for ethanol synthesis toward the fatty alcohol synthesis from fatty acid methyl

624   esters, we confirmed the analysis carried out at macroscopic level based on experimental

625   results.

626

633

634   **Authorship**

635   **V.K.D.** Conceived and designed the study; conceptualized, supervised and analyzed the

636   data; and wrote the first draft of the manuscript. **C.A.F.** Conceptualized and supervised

637   theoretical research (DFT) and analyzed the data. **A.V.O.** Carried out the experimental

638   and theoretical research and analyzed the data. All authors contributed to and approved

639   the final draft of the manuscript.

640

641 **Declaration of Competing Interest**

642 The authors declare that they have no known competing financial interests or personal

643 relationships that could have appeared to influence the work reported in this paper.

644

645 **References**

646 Barroso Joaquin's Blog. Available from: https://joaquinbarroso.com/ [accessed 3rd

647   February 2021].

648 Bernal J.P., Railsback L.B., Introducción a la Tabla Periódica de los Elementos y sus

649   Iones para Ciencias de la Tierra, Rev. Mex. Ciencias Geológicas. 2008; 25:236-246.

650 Brown H.C., Narasimhan S., Choi Y.M., Selective Reductions. 30. Effect of Cation and

651   Solvent on the Reactivity of Saline Borohydrides for Reduction of Carboxylic Esters.

652   Improved Procedures for the Conversion of Esters to Alcohols by Metal Borohydrides,

653   J. Org. Chem. 1982; 47:4702-4708. https://doi.org/10.1021/jo00145a018.

654 Demirci U.B., Akdim O., Andrieux J., Hannauer J., Chamoun R., Miele P., Sodium

655   Borohydride Hydrolysis as Hydrogen Generator: Issues, State of the Art and

656   Applicability Upstream from a Fuel Cell, Fuel Cells. 2010; 10:335-350.

657   https://doi.org/10.1002/fuce.200800171.

658 De Oliveira K., Pouilloux Y., Barrault J., Selective Hydrogenation of Methyl Oleate into

659   Unsaturated Alcohols in the Presence of Cobalt–Tin Supported over Zinc Oxide

660   Catalysts, J. Catal. 2001; 204:230-237. https://doi.org/10.1006/jcat.2001.3378.

661 De Oliveira Vigier K., Pouilloux Y., Barrault J., High efficiency CoSn/ZnO catalysts for

662   the hydrogenation of methyl oleate, Catal. Today. 2012; 195:71-75.

663   https://doi.org/10.1016/j.cattod.2012.04.027.

664 Devia I.C.R., Determinación del estado de transición en la reacción de oxidación del n-

665   heptano con el catalizador [MnAcO($C_{16}H_{14}N_2O_2$)] mediante la exploración de la

666   superficie de energía potencial, Universidad de Ciencias Aplicadas y Ambientales,

667   2018.

668   Díez V.K., Apesteguía C.R., Di Cosimo J.I., Effect of the chemical composition on the

669   catalytic performance of Mg_yAlO_x catalysts for alcohol elimination reactions, J. Catal.

670   2003; 215:220-233. https://doi.org/10.1016/S0021-9517(03)00010-1.

671   Echeverri D.A., Rios L.A., Marín J.M., Síntesis de alcoholes grasos insaturados a partir

672   de metilésteres grasos usando catalizadores a base de rutenio y estaño soportados sobre

673   alúmina, Ing. e Investig. 2011; 31:74-82.

674   Fernandes V.R., Pinto A.M.F.R., Rangel C.M., Hydrogen production from sodium

675   borohydride in methanol-water mixtures, Int. J. Hydrogen Energy. 2009; 35:9862-

676   9868. https://doi.org/10.1016/j.ijhydene.2009.11.064.

677   Foresman J.B., Frisch A., Exploring Chemistry With Electronic Structure Methods, 3rd

678   ed., Gaussian Inc., Wallingford, CT; 2015.

679   Frisch M.J., Trucks G.W., Schlegel H.B., Scuseria G.E., Robb M.A., Cheeseman J.R.,

680   Scalmani G., Barone V., Petersson G.A., Nakatsuji H., Li X., Caricato M., Marenich

681   A., Bloino J., Janesko B.G., Gomperts R., Mennucci B., Hratchian H.P., Ortiz J.V.,

682   Izmaylov A.F., Sonnenberg J.L., Williams-Young D., Ding F., Lipparini F., Egidi F.,

683   Goings J., Peng B., Petrone A., Henderson T., Ranasinghe D., Zakrzewski V.G., Gao

684   J., Rega N., Zheng G., Liang W., Hada M., Ehara M., Toyota K., Fukuda R., Hasegawa

685   J., Ishida M., Nakajima T., Honda Y., Kitao O., Nakai H., Vreven T., Throssell K.,

686   Montgomery J.A. Jr., Peralta J.E., Ogliaro F., Bearpark M., Heyd J.J., Brothers E.,

687   Kudin K.N., Staroverov V.N., Keith T., Kobayashi R., Normand J., Raghavachari K.,

688   Rendell A., Burant J.C., Iyengar S.S., Tomasi J., Cossi M., Millam J.M., Klene M.,

689   Adamo C., Cammi R., Ochterski J.W., Martin R.L., Morokuma K., Farkas O.,

690 Foresman J.B., Fox D.J., Gaussian 09 (Revision A.02), 2016.
691 https://gaussian.com/glossary/g09/.

692 Inmanee T., Pinthong P., Jongsomjit B., Effect of Calcination Temperatures and Mo
693 Modification on Nanocrystalline (γ-χ)-Al_2O_3 Catalysts for Catalytic Ethanol
694 Dehydration, J. Nanomater. 2017; Article ID 5018384:9 pages.
695 https://doi.org/10.1155/2017/5018384.

696 Kaya M., Bekirogullari M., Investigation of Hydrogen Production from Sodium
697 Borohydride Methanolysis in the Presence of Al_2O_3/Spirulina Platensis Supported Co
698 Catalyst, Eur. J. Sci. Technol. 2019; 16:69-76. https://doi.org/10.31590/ejosat.549911.

699 Lee C., Yang W., Parr R.G., Development of the Colle-Salvetti correlation-energy
700 formula into a functional of the electron density, Phys. Rev. B. 1988; 37:785-789.
701 https://doi.org/https://doi.org/10.1103/PhysRevB.37.785.

702 Lo C.F., Karan K., Davis B.R., Kinetic Studies of Reaction between Sodium Borohydride
703 and Methanol, Water, and Their Mixtures, Ind. Eng. Chem. Res. 2007; 46:5478-5484.
704 https://doi.org/10.1021/ie0608861.

705 Mazzieri V.A., Sad M.R., Vera C.R., Pieck C.L., Prearation and characterization of Ru-
706 Sn/Al_2O_3 catalysts for the hydrogenation of fatty acid methyl esters, Quim. Nova.
707 2010; 33:269-272. https://doi.org/10.1590/S0100-40422010000200007.

708 McKee J.R., Zanger M., Chiariello C., McKee J.A., Dorfner W., Fasella E., Koo Y.,
709 Semimicro/Microscale Adaptation of the Cobalt Chloride/Sodium Borohydride
710 Reduction of Methyl Oleate, J. Chem. Educ. 2019; 96:772-775.
711 https://doi.org/10.1021/acs.jchemed.8b00222.

712 Miya B. Method of producing copper-iron-aluminum catalysts. US4252689 (Patent),
713 1981.

714   Narasimhan C.S., Deshpande V.M., Ramnarayan K., Selective Hydrogenation of Methyl

715   Oleate to Oleyl Alcohol on Mixed Ruthenium-Tin Boride Catalysts, Appl. Catal. 1989;

716   48:L1-L6. https://doi.org/10.1016/S0166-9834(00)80260-2.

717   Noweck K., Production, Technologies and Applications of Fatty Alcohols, Work. Fats

718   Oils as Renew. Feed. Chem. Ind. 2011:1-9.

719   Ocon J.D., Tuan T.N., Yi Y., De Leon R.L., Lee J.K., Lee J., Ultrafast and stable

720   hydrogen generation from sodium borohydride in methanol and water over Fe-B

721   nanoparticles, J. Power Sources. 2013; 243:444-450.

722   https://doi.org/10.1016/j.jpowsour.2013.06.019.

723   Pouilloux Y., Piccirilli A., Barrault J., Selective hydrogenation into oleyl alcohol of

724   methyl oleate in the presence of Ru-Sn/Al$_2$O$_3$ catalysts, J. Mol. Catal. A Chem. 1996;

725   108:161-166. https://doi.org/10.1016/1381-1169(96)00010-6.

726   Pouilloux Y., Autin F., Piccirilli A., Guimon C., Barrault J., Preparation of oleyl alcohol

727   from the hydrogenation of methyl oleate in the presence of cobalt-tin catalysts, Appl.

728   Catal. A Gen. 1998; 169:65-75. https://doi.org/10.1016/S0926-860X(97)00344-X.

729   Pouilloux Y., Autin F., Barrault J., Selective hydrogenation of methyl oleate into

730   unsaturated alcohols relationships between catalytic properties and composition of

731   cobalt-tin catalyst, Catal. Today. 2000; 63:87-100.

732   https://doi.org/https://doi.org/10.1016/S0920-5861(00)00448-X.

733   Rajeswara Rao Y., Pantulu A.J., Lakshminarayana G., Reduction of Fatty Acid Methyl

734   Esters with Sodium Borohydride-t-Butanol-Methanol, Fat Sci. Technol. 1987; 89:398-

735   400. https://doi.org/https://doi.org/10.1002/lipi.19870891006

736   Rieke R.D., Thakur D.S., Roberts B.D., White G.T., Fatty Methyl Ester Hydrogenation

737   to Fatty Alcohol Part I: Correlation Between Catalyst Properties and

738   Activity/Selectivity, J. Am. Oil Chem. Soc. 1997; 74:333-339.

739   https://doi.org/10.1007/s11746-997-0088-y.

740   Rieke R.D., Thakur D.S., Roberts B.D., White G.T., Fatty Methyl Ester Hydrogenation

741   to Fatty Alcohol Part II: Process Issues, J. Am. Oil Chem. Soc. 1997; 74:341-345.

742   https://doi.org/10.1007/s11746-997-0089-x.

743   Sad M.R., Mazzieri V.A., Vera C.R., Pieck C.L., Hidrogenación selectiva de metil ésteres

744   de ácidos grasos para obtención de alcoholes grasos. I. Perspectivas actuales,

745   catalizadores y mecanismos de reacción, Av. En Química, 2007:17-24.

746   Sánchez M.A., Mazzieri V.A., Oportus M., Reyes P., Pieck C.L., Influence of Ge content

747   on the activity of Ru-Ge-B/Al_2O_3 catalysts for selective hydrogenation of methyl

748   oleate to oleyl alcohol, Catal. Today. 2013; 213:81-86.

749   https://doi.org/10.1016/j.cattod.2013.02.028.

750   Soai K., Oyamada H., Ookawa A., Sodium Borohydride-t-butyl Alcohol-Methanol as an

751   Efficient System for the Selective Reduction of Esters, Synth. Commun. 1982; 12:463-

752   467. https://doi.org/10.1080/00397911.2011.574329.

753   Soai K., Oyamada H., Takase M., Ookawa A., Practical Procedure for the Chemoselective

754   Reduction of Esters by Sodium Borohydride. Effect of the Slow Addition of Methanol,

755   Bull. Chem. Soc. Jpn. 1984; 57:1948-1953.

756   https://doi.org/https://doi.org/10.1246/bcsj.57.1948.

757   Tahara K., Tsuji H., Kimura H., Okazaki T., Itoi Y., Nishiyama S., Tsuruya S., Masai M.,

758   Liquid-phase hydrogenation of dicarboxylates catalyzed by supported Ru-Sn catalysts,

759   Catal. Today. 1996; 28:267-272. https://doi.org/https://doi.org/10.1016/0920-

760   5861(95)00247-2.

761   Toba M., Tanaka S., Niwa S., Mizukami F., F. Koppány F., Guczi L., Cheah K.Y., Tang

762   T.S., Synthesis of alcohols and diols by hydrogenation of carboxylic acids and esters

763   over Ru–Sn–Al$_2$O$_3$ catalysts, Appl. Catal. A Gen. 1999; 189:243-250.

764   https://doi.org/10.1016/S0926-860X(99)00281-1.

765   Vallejo Orrego A., Ferretti C.A., Díez V.K., Reduction of Vegetable Oil-Derived Fatty

766   Acid Methyl Esters toward Fatty Alcohols without the Supply of Gaseous H$_2$, JAOCS,

767   J. Am. Oil Chem. Soc. 2020; 97:1029-1042. https://doi.org/10.1002/aocs.12375.

768   Xin Z., Wei G., Zhang L., Gao L., Li Z., Zhao W., Partial hydrogenation of fatty acid

769   methyl esters under mild conditions using sodium borohydride as hydrogen donor,

770   Fuel. 2021; 299: Article ID 120877. https://doi.org/10.1016/j.fuel.2021.120877.

771   Xu Y., Wei Y., CeCl$_3$-Catalyzed Reduction of Methyl Esters of Carboxylic Acids to

772   Corresponding Alcohols with Sodium Borohydride, Synth. Commun. 2010; 40:3423-

773   3429. https://doi.org/10.1080/00397910903457233.

774   Yoshino K., Kajiwara Y., Takaishi N., Inamoto Y., Tsuji J., Hydrogenation of Carboxylic

775   Acids by Rhenium-Osmium Bimetallic Catalyst, J. Am. Oil Chem. Soc. 1990; 67:21-

776   24. https://doi.org/10.1007/bf02631383.

777

778

779

780

781

782

783

784

785

786

787

788 **Captions to Figures and Schemes**

789

790 **Scheme 1.** Reaction mechanism for fatty acid methyl ester reduction using methanol as

791 proton donor and sodium borohydride as hydride donor.

792

793 **Scheme 2.** Stoichiometry of oleyl alcohol (OA) synthesis reaction from methyl oleate,

794 methanol and sodium borohydride.

795

796 **Scheme 3.** Possible mechanisms involved in the methyl acetate reduction reaction used

797 for DFT calculations.

798

799 **Figure 1.** Diffractograms obtained on xMAl samples.

800

801 **Figure 2.** CO_2 TPD (A) and NH_3 TPD (B) profiles for xMAl solids.

802

803 **Figure 3.** Relation between n_a and q/r for xMAl catalysts.

804

805 **Figure 4.** Effect of reaction temperature during methyl oleate conversion to oleyl

806 alcohol (T = 308 K, 320 K, 333 K; FAME/NaBH$_4$ molar ratio = 0.28; methanol/NaBH$_4$

807 molar ratio = 6.0; NaBH$_4$ as reducing solid).

808

809 **Figure 5.** Effect of varying FAME/NaBH$_4$ molar ratio during methyl oleate conversion

810 to oleyl alcohol (T = 333 K; methanol/NaBH$_4$ molar ratio = 6.0; NaBH$_4$ as reducing

811 solid).

812

813   **Figure 6. Figure 6.** MO conversion as a function of reaction time on xMAl catalysts (T

814   = 333 K; MO/NaBH$_4$ molar ratio = 0.11; methanol/NaBH$_4$ molar ratio = 6.0; NaBH$_4$/MAl

815   as reducing solid).

816

817   **Figure 7.** Relation between r^0_{MO} and n_b (A) and, r^0_{MO} and q/r and n_a (B) for xMAl

818   catalysts (T = 333 K; MO/NaBH$_4$ molar ratio = 0.11; methanol/NaBH$_4$ molar ratio =

819   6.0).

820

821   **Figure 8.** Different optimized initial geometries (A), transitions states (A) and

822   intermediates (C) found for methyl acetate reduction reaction obtained from DFT

823   calculations.

824

825   **Figure 9.** Reaction energy profile for methyl acetate reduction toward ethanol formation

826   obtained from DFT calculations.

827

828

829

830

831

832

833

834

835

836

Table 1. Chemical, textural, structural and acid-base characterization of xMAl catalysts.

Catalyst	Metal content, x^a (wt. %)	Textural properties			Acid-base properties			Structural phases detected by XRD
		SA^b (m^2/g)	Pore volume, Vg (cm^3/g)	Pore size, dp (Å)	n_b^c (µmol/g)	n_a^d (µmol/g)	Ionic potential, q/r	
CeAl	7.0	173	0.41	95.2	16	111	3.96	CeO$_2$, γ-Al$_2$O$_3$
FeAl	7.7	53	0.10	76.7	9	128	4.62	Fe$_2$O$_3$, AlFeO$_3$, γ-Al$_2$O$_3$
MoAl	8.9	128	0.27	84.1	12	977[e]	9.68	γ-Al$_2$O$_3$
γ-Al$_2$O$_3$	-	230	-	-	19	24	-	γ-Al$_2$O$_3$

[a] by ICP; [b] BET surface areas; [c] by TPD of CO$_2$; [d] by TPD of NH$_3$; [e] from reference [19]

Table 2. Non-catalytic and catalytic results obtained during methyl oleate reduction using $NaBH_4$.

Catalyst	Reaction conditions			Results obtained during MO reduction		
	Reaction temperature (K)	MO/NaBH$_4$ molar ratio	Methanol/NaBH$_4$ molar ratio	S_{OA} [a] (%)	X_{MO} or Y_{OA} [b] (%)	r^0_{MO} [c] (mol/hg)
-	308	0.28	6.0	100.0	31.9	-
-	320	0.28	6.0	100.0	40.2	-
-	333	0.28	6.0	100.0	58.6	-
-	333	0.11	6.0	100.0	93.9	-
-	333	0.72	6.0	100.0	21.4	-
γ-Al$_2$O$_3$	333	0.11	6.0	100.0	53.0	0.16
CeAl	333	0.11	6.0	100.0	48.8	0.16
FeAl	333	0.11	6.0	100.0	58.7	0.18
MoAl	333	0.11	6.0	100.0	81.6	0.20

[a] during the whole 6-hour experiment; [b] at t = 6 h; [c] Initial MO conversion rate (at t = 0).
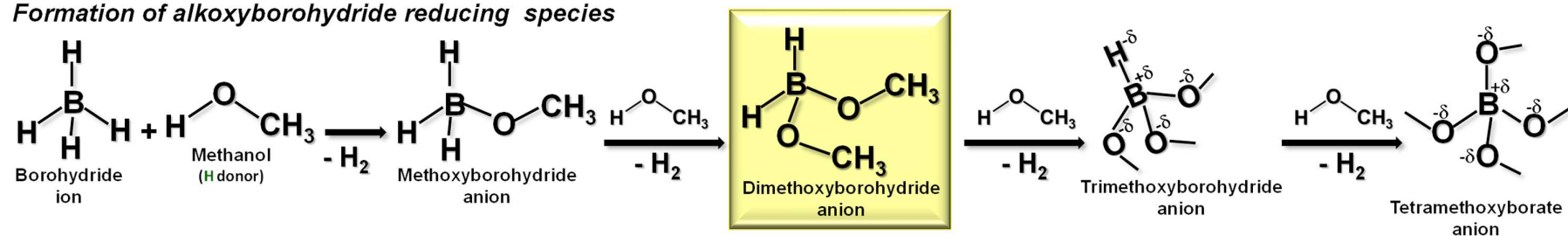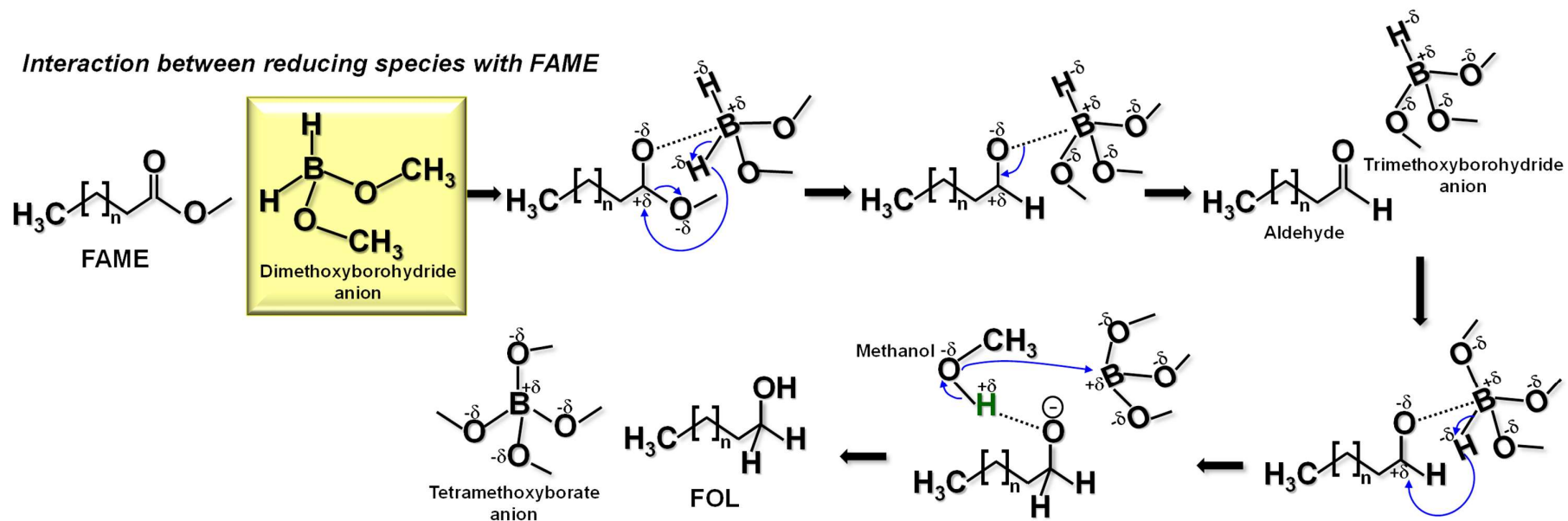
Scheme 1. Reaction mechanism for fatty acid methyl ester reduction using methanol as proton donor and sodium borohydride as hydride donor.

$$CH_3\text{-}(CH_2)_7\text{-}CH=CH\text{-}(CH_2)_7\text{-}\overset{\overset{\displaystyle O}{\|}}{C}\text{-}O\text{-}CH_3 \ + \ NaBH_4 \ + \ 3\ CH_3\text{-}O\text{-}H \longrightarrow CH_3\text{-}(CH_2)_7\text{-}CH=CH\text{-}(CH_2)_7\text{-}CH_2\text{-}OH \ + \ NaB(OCH_3)_4 \ + \ 2\ H_2$$

Methyl oleate   Sodium   Methanol   Oleyl alcohol   Sodium
(MO)   borohydride   (OA)   tetramethoxyborate
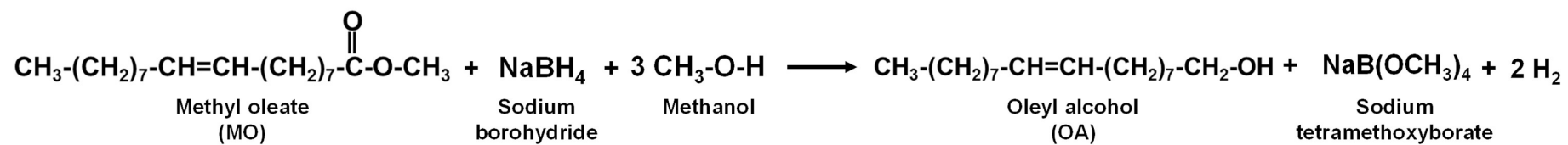
Scheme 2. Stoichiometry of oleyl alcohol (OA) synthesis reaction from methyl oleate, methanol and sodium borohydride.
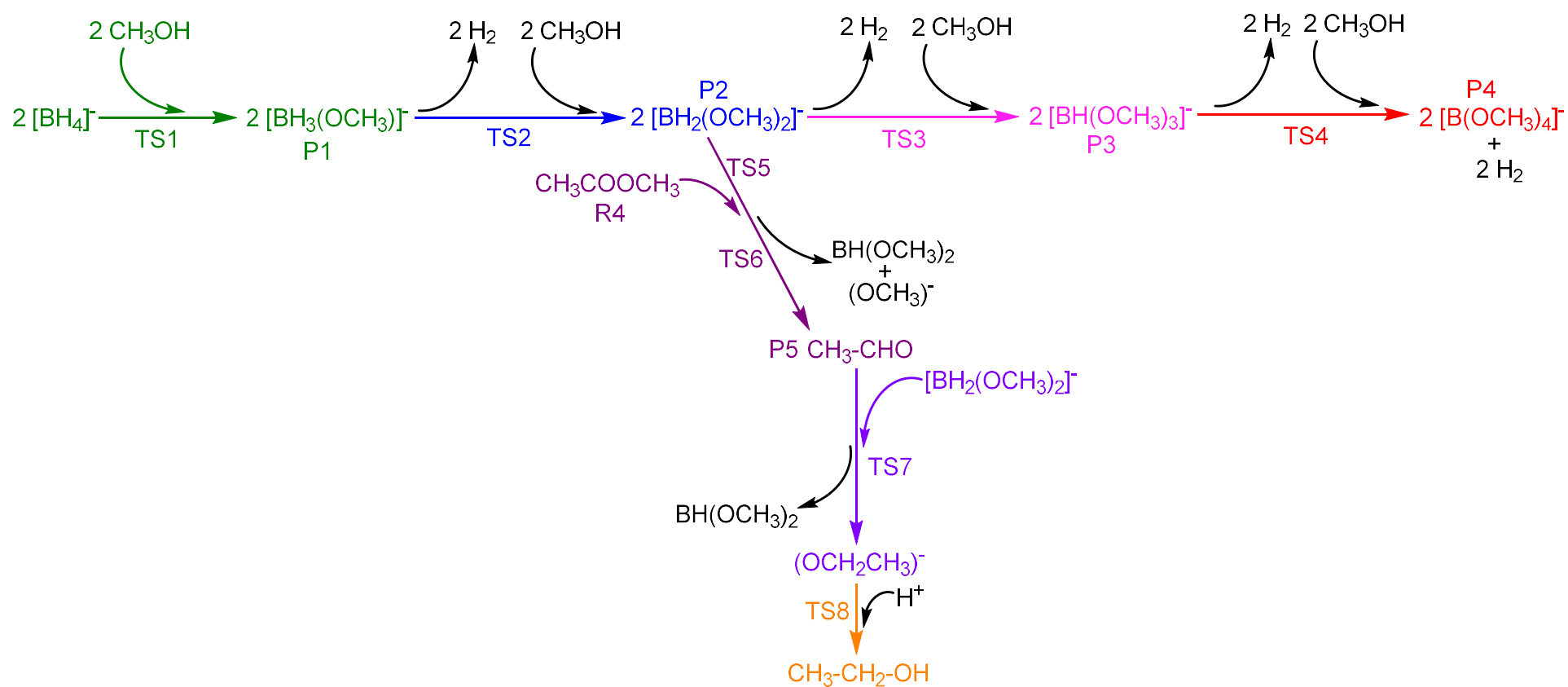
Scheme 3. Possible mechanisms involved in the methyl acetate reduction reaction used for DFT calculations.
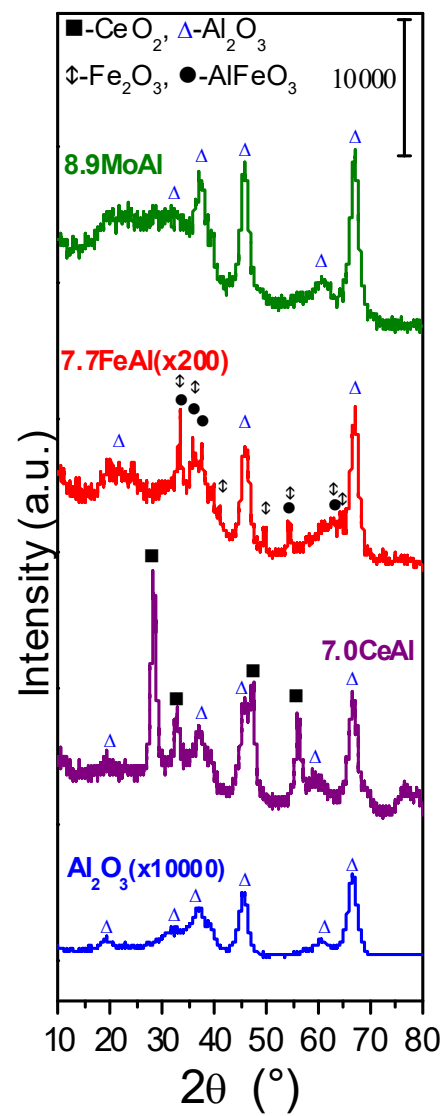
Figure 1. Diffractograms obtained on *x*MAl samples.
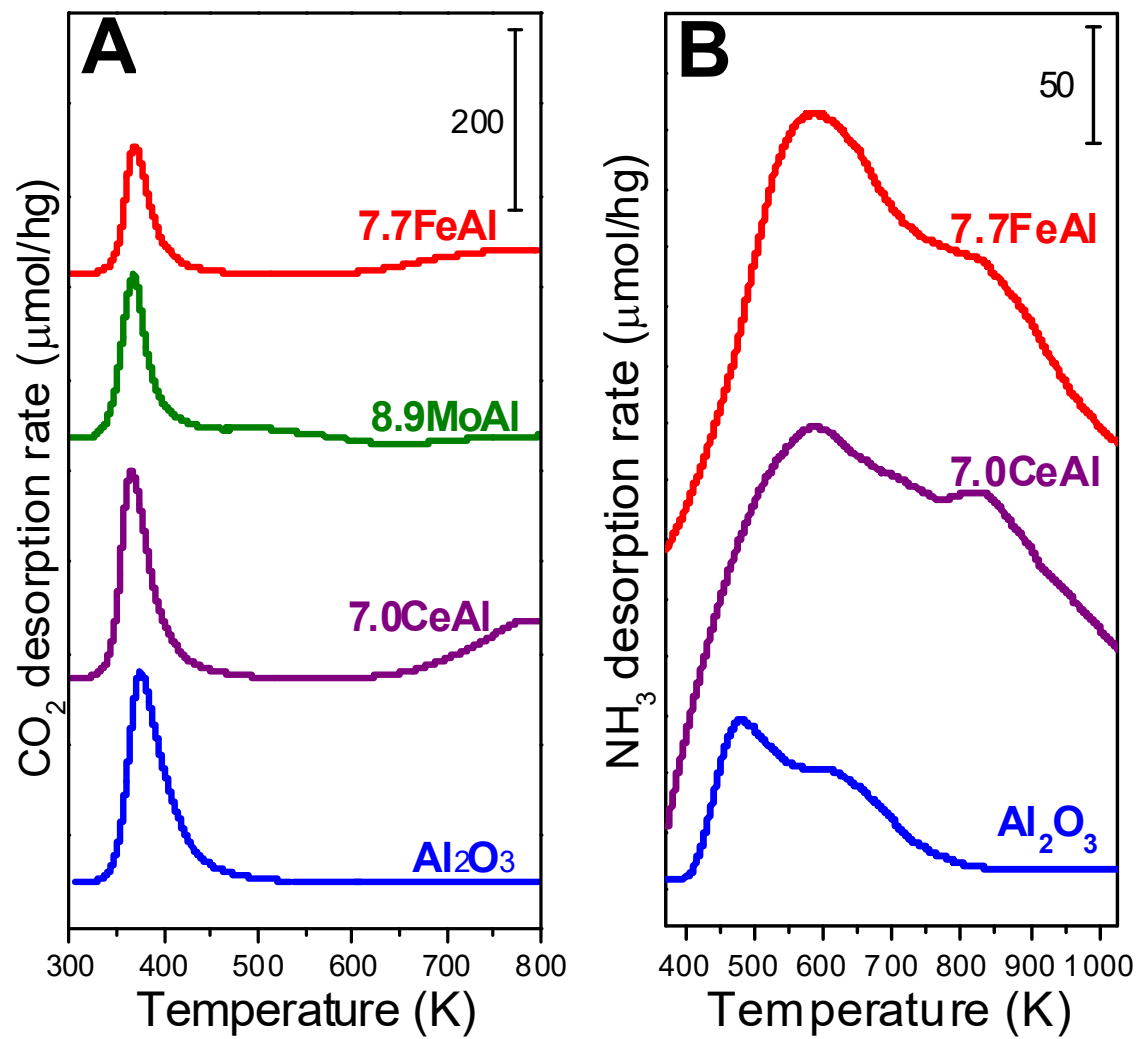
Figure 2. CO_2 TPD (A) and NH_3 TPD (B) profiles for xMAl solids.
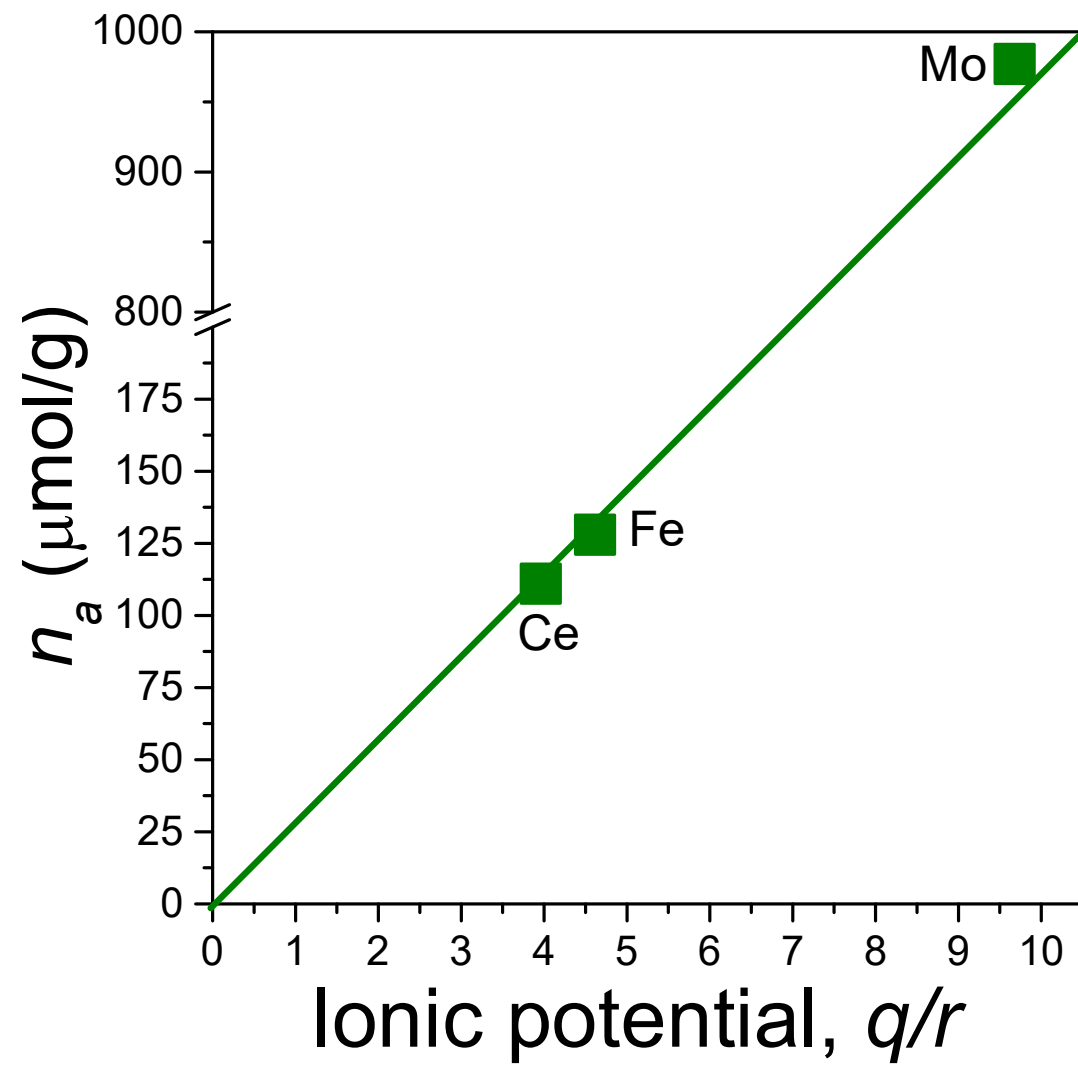
Figure 3. Relation between n_a and q/r for xMAl catalysts.
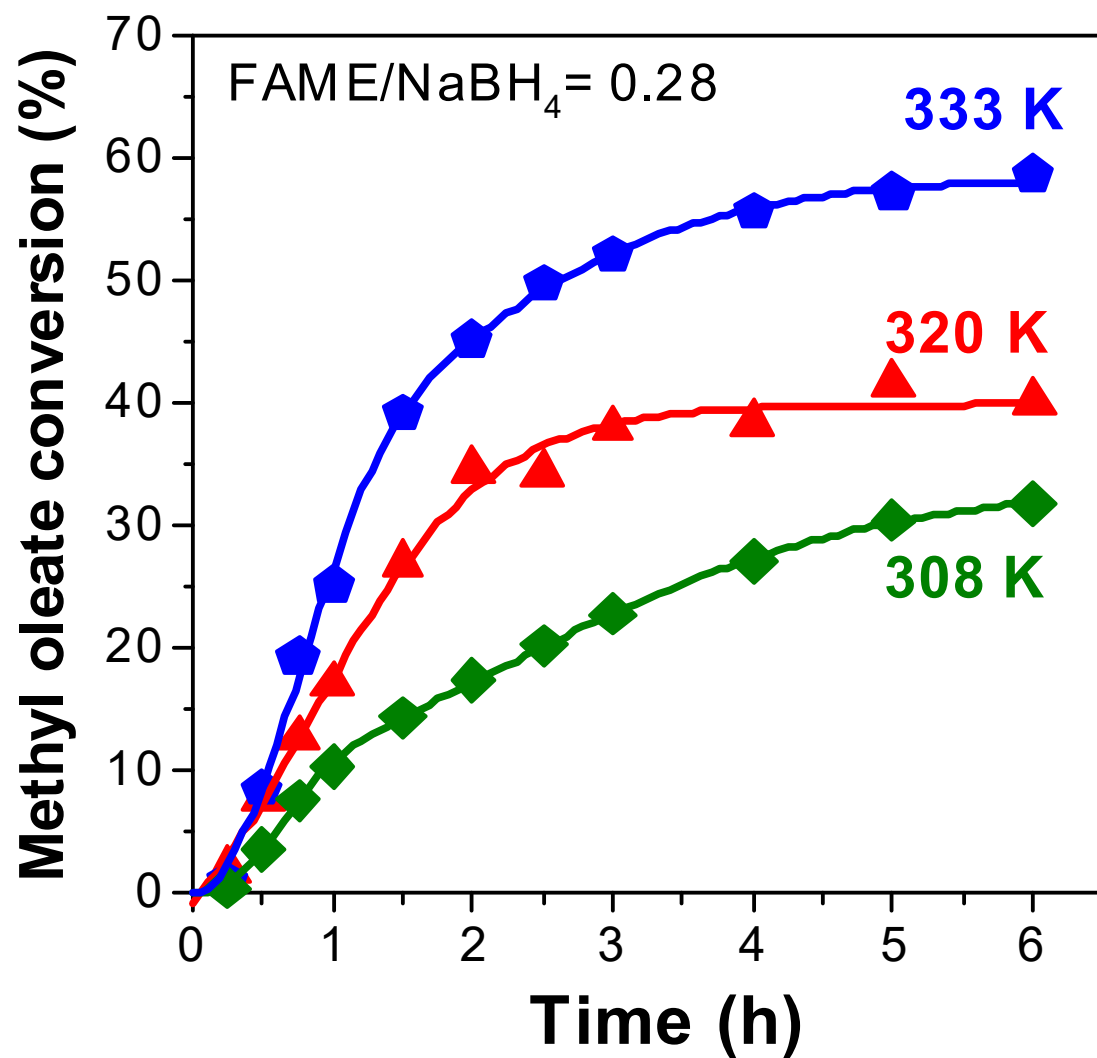
Figure 4. Effect of reaction temperature during methyl oleate conversion to oleyl alcohol (T = 308 K, 320 K, 333 K; FAME/NaBH₄ molar ratio = 0.28; methanol/NaBH₄ molar ratio = 6.0; NaBH₄ as reducing solid).
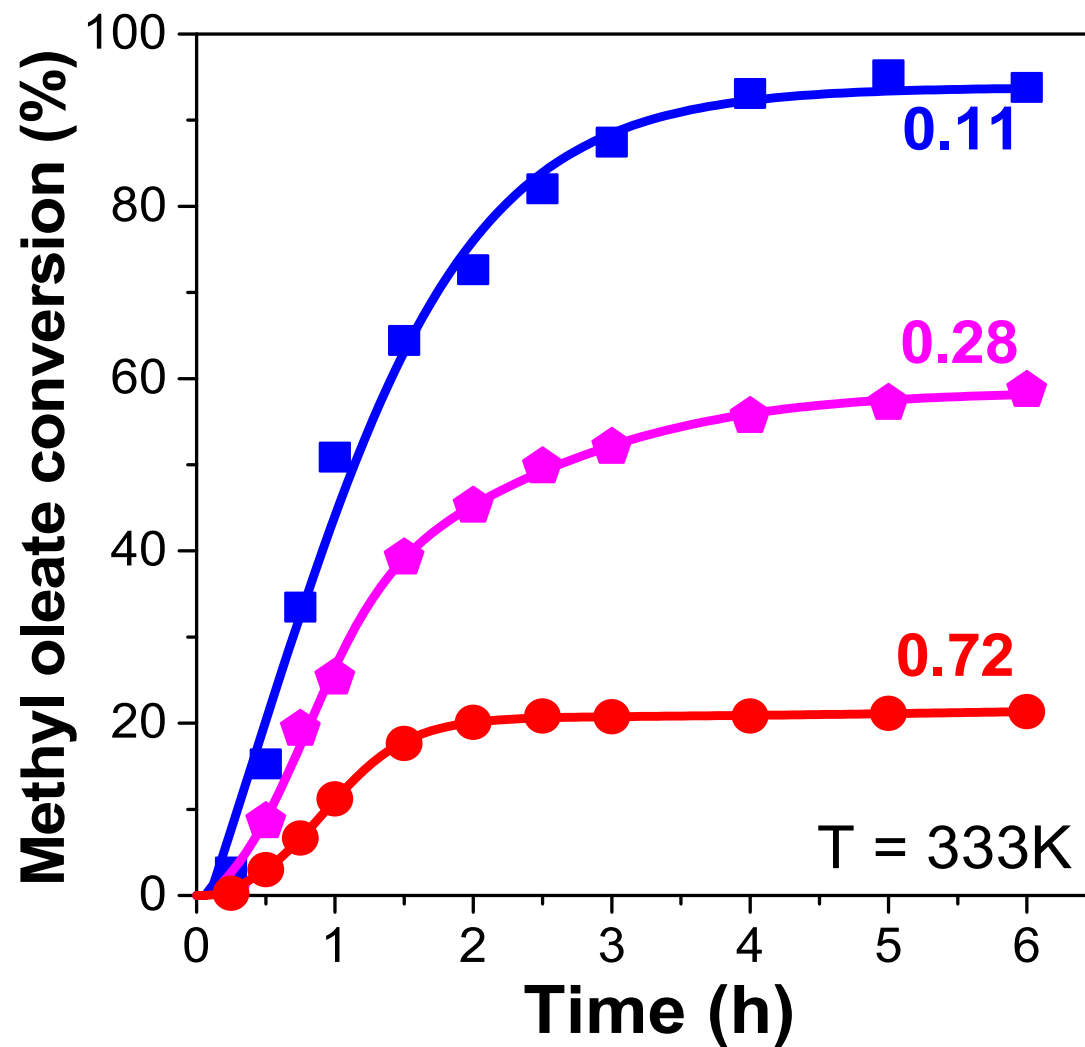
Figure 5. Effect of varying FAME/NaBH$_4$ molar ratio during methyl oleate conversion to oleyl alcohol (T = 333 K; methanol/NaBH$_4$ molar ratio = 6.0; NaBH$_4$ as reducing solid).
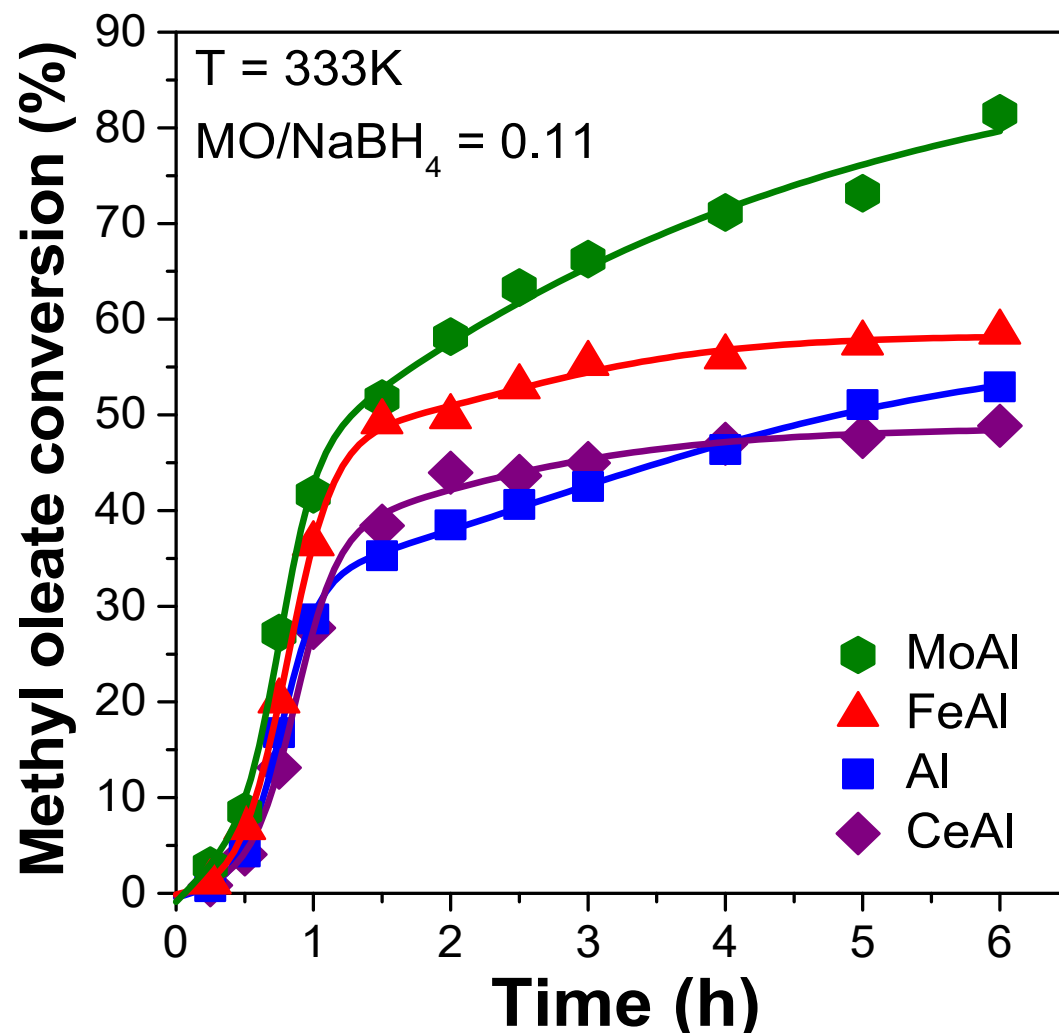
Figure 6. MO conversion as a function of reaction time on xMAl catalysts (T = 333 K; $MO/NaBH_4$ molar ratio = 0.11; methanol/$NaBH_4$ molar ratio = 6.0; $NaBH_4$/MAl as reducing solid).
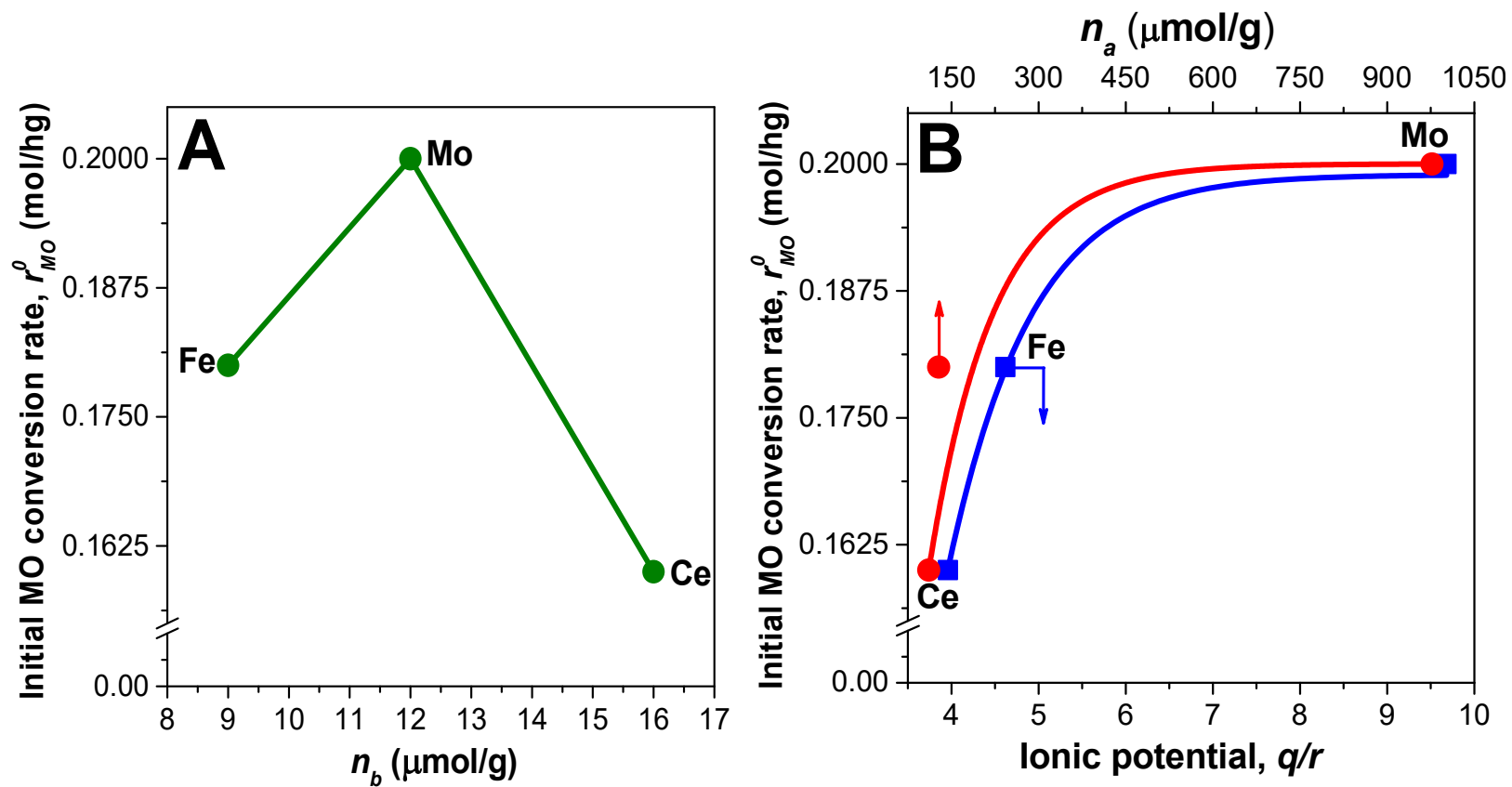
Figure 7. Relation between r^0_{MO} and n_b (A) and, r^0_{MO} and q/r and n_a (B) for xMAl catalysts (T = 333 K; MO/NaBH$_4$ molar ratio = 0.11; methanol/NaBH$_4$ molar ratio = 6.0).
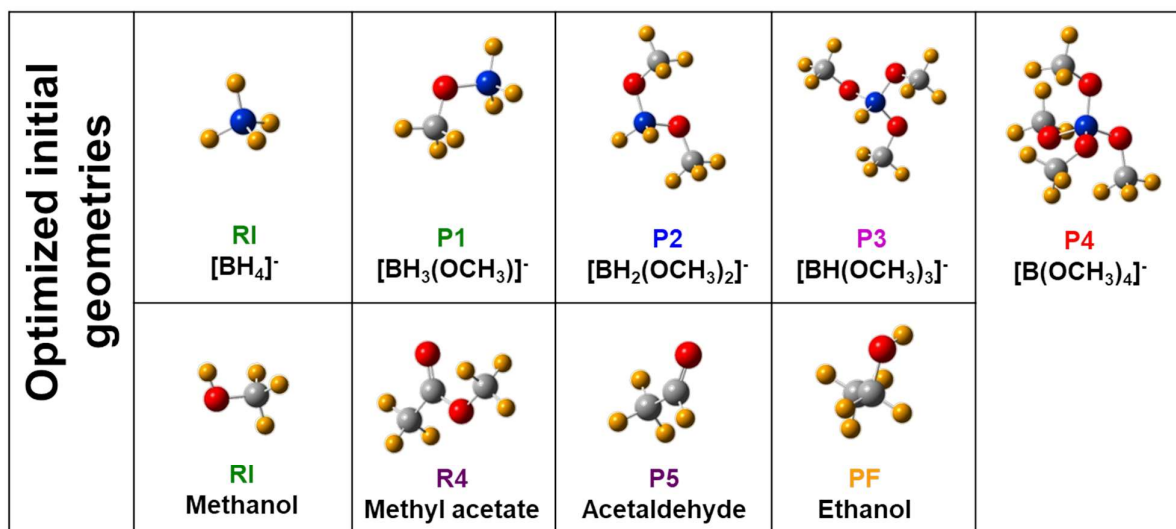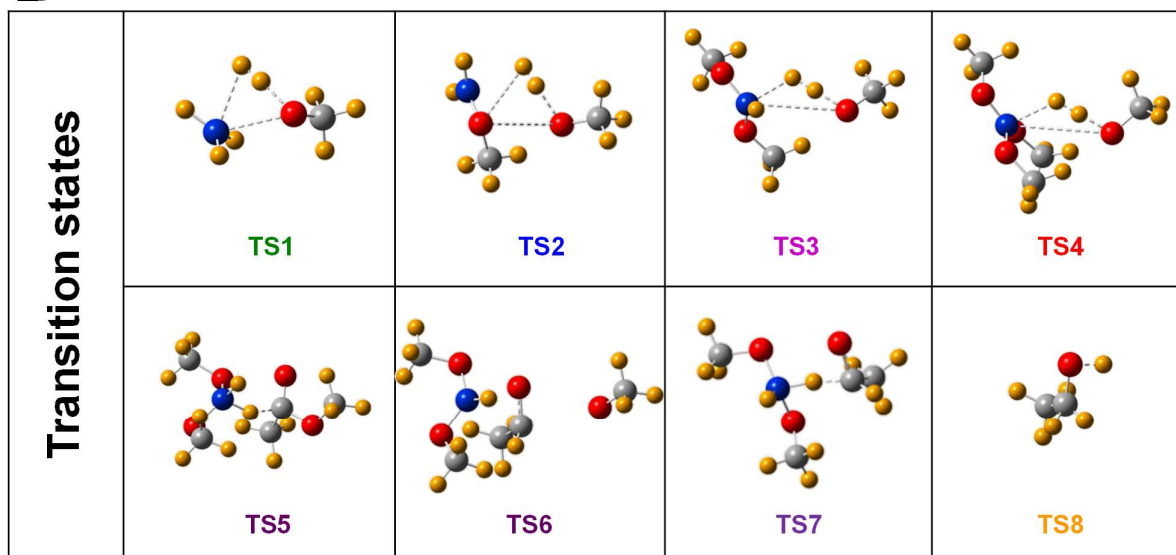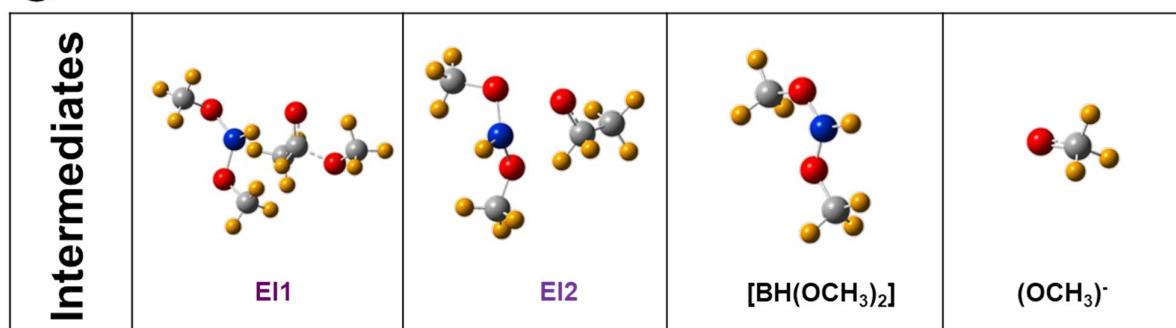
Figure 8. Different optimized initial geometries (A), transitions states (A) and intermediates (C) found for methyl acetate reduction reaction obtained from DFT calculations.
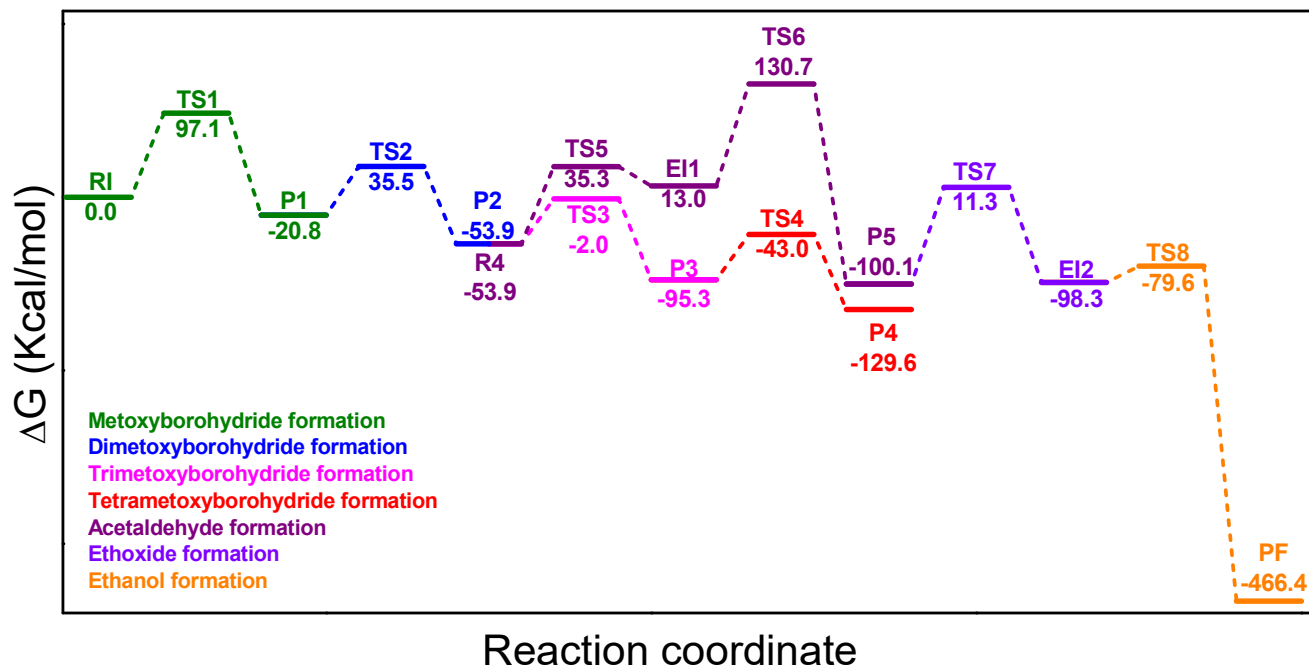
Figure 9. Reaction energy profile for methyl acetate reduction toward ethanol formation obtained from DFT calculations.